BULGARIAN CHEMICAL COMMUNICATIONS

2025 Volume 57 / Number 1

Journal of the Chemical Institutes
of the Bulgarian Academy of Sciences
and of the Union of Chemists in Bulgaria

Anniversary

Prof. Christo Balarew's 90th anniversary

Prof. Christo Balarew, PhD, DSc, has turned 90. He is an eminent scientist, lecturer, public figure, member of organizational and scientific committees of international scientific forums, guest professor and lecturer at foreign universities, such as the University Claude Bernard in Lyon, France, the University of Valladolid, Spain, the Mining Academy Freiberg and the University of Siegen, Germany, the University of Colorado in Boulder, USA, the McMaster University in Hamilton, Ontario, Canada, the University of Witwatersrand, Johannesburg, South Africa, etc. During the period 1997-2001, he was Deputy Minister of Education and Science.

He has been a president of the National Committee at the International Union for Pure and Applied Chemistry for the period 1998/2022.

He was born on June 23, 1934 in Sofia. In 1957, he graduated in chemistry from the Faculty of Physics and Mathematics of Sofia University. He worked for 2 years as a high school teacher, then in 1959 entered the then Chemical Institute of the Bulgarian Academy of Sciences. In 1967 he was elected Associate Professor at the newly established Higher Chemical-Technical Institute - Burgas where he headed the Department of Inorganic Chemistry. In the meantime, as a part-time doctoral student, he defended his PhD thesis at the Mining Academy Freiberg, Germany (1969). In 1972 he returned to Sofia as Associate Professor at the Institute of General and Inorganic Chemistry of the Bulgarian Academy of Sciences, and in 1988 he was elected Professor and Head of the Laboratory of Inorganic Salts at the institute, in which scientific activity he still participates today. During the years 1976-1978 he was a scholarship holder of the Alexander von Humboldt Foundation. In 1983 he defended his Doctor of Chemical Sciences thesis on the topic "Regularities of the equilibrium formation of mixed crystals and double salts from three-component water-salt systems".

The scientific studies of Prof. Chr. Balarew are in the field of solubility and crystallization processes of salts in multicomponent model and natural systems. In aqueous solutions, the ions of salts are always hydrated, forming complexes with each other. The latter are grouped into complex associates of different sizes depending on the composition of the solutions, the concentrations of the salts and the temperature. Balarew's contribution is in the application of Pearson's concept of "hard and soft" Lewis acids and bases with a view to determine which are the preferred metal-ligand bonds in a given system. On this knowledge, by applying Pauling's rules for building coordination polyhedra, Balarew predicted the composition and structure of the complexes prevailing in the respective solution. Postulating that the kinetics of both nucleation and crystallization depend on the structural analogy between the complexes and fragments of the structure of the crystallizing phase prevailing in the solution, Balarew explained a number of phenomena, e.g., the kinetics of nucleation, and the oversaturation ability of the solutions. The classification of the latter according to this characteristic, explains Ostwald's Rule of Stages for the crystallization of metastable phases, throws light on the difference in the sequence of crystallization upon evaporation of the water from multicomponent salt solutions under natural or laboratory conditions, from the sequence required by thermodynamics, and offers explanations for the structure of mineral evaporite deposits.

Again on the basis of Pearson's concept of "hard and soft" Lewis acids and bases, Balarew, together with R. Duhlev, explained the formation of double salts and developed a procedure for predicting their composition and structure, a problem that no one had tackled before them.

A significant contribution of Balarew is his theory of isomorphic and isodimorphic co-crystallization. Balarew's proposed formula for the distribution coefficient of salt 1 and salt 2 between the solid and liquid phases (D_{21}) during co-crystallization is:

$$D_{2/1} = \left[\frac{M_{1,0}}{M_{2,0}}\right]^2 \cdot \exp \frac{a \cdot f\left(\frac{\Delta R}{R}\right) + b \cdot \varphi(\Delta\varepsilon) + c \cdot \psi(\Delta s)}{RT}$$

where M_1 and M_2 are the solubilities of salt 1 and salt 2 in pure water at the corresponding temperature, while

$a \cdot f\left(\frac{\Delta R}{R}\right)$ $b \cdot \varphi(\Delta\varepsilon)$ and $c \cdot \psi(\Delta s)$

take into account the changes in Gibbs free energy that occur during co-crystallization due to changes in the crystal structure, changes in the energies of the metal-ligand bonds, and as a result of the stabilization energy in the crystal field.

In isovalent-isomorphous cocrystallization, the numerator in the exponential term can be assumed to be 0 and the formula simplifies to:

$$D_{2/1} = \left(\frac{M_1}{M_2}\right)^2$$

The numerator in the exponential term represents the change in Gibbs free energy upon transition of component 1 with crystal structure I to crystal structure II (GI→II). Using this formula, Balarew also proposed a method for determining this free energy from experimental data for the distribution coefficient in the immediate vicinity of the eutonic points of the solubility diagrams of the corresponding ternary systems.

The scientific achievements of Christo Balarew are published in over 200 scientific papers, most of which in renowned international journals. Prof. Balarew is also the author of 5 books and monographs and several dozen popular science articles. Balarew's applied research, based on the obtained fundamental results, led to the development of a dozen technologies for obtaining chemical products with reagent purity, for the synthesis of new materials, for the recovery of useful components from natural raw materials and industrial waste products by hydrometallurgical means. He participated in the implementation of over 30 international, European and national projects. He created an Experimental and Production Base in Burgas for the utilization of the chemical resources of the Black Sea, which even today enables chemists to conduct pilot studies for testing and implementing environmentally friendly technologies. He himself has developed technologies and original methods, protected by 19 copyright certificates and 1 patent. During the period 1972-1994, he organized a series (7 in total) of national scientific conferences in Sunny Beach on the utilization of the chemical resources of the Black Sea. In July 2002 in Varna the 10th International IUPAC Symposium on Solubilities with the participation of over 200 scientists from 30 countries from five continents, was held under the chairmanship of Prof. Balarew.

In the field of inorganic chemistry education, Prof. Balarew has left a remarkable trail. He managed to create in his students love for chemistry, teached them honesty and dedication to science. His students at the Chemical-Technical Institute-Burgas, the Chemical-Technical Institute -Sofia, the Plovdiv University and the Faculty of Chemistry of Sofia University defined his lectures as some of the most interesting ones. On the basis of his scientific ideas he has guided the scientific development and growth of 13 successfully defended PhD students. To this day, he pays special attention to the younger generation. To encourage young researchers in their early careers, he established two annual awards - the national award of the Union of Chemists in Bulgaria "Prosperous Young Scientist in the Field of Inorganic Chemistry" and the award of the International Union of Pure and Applied Chemistry (IUPAC) "Young Scientist Working in the Field of Solubility and Equilibrium Data".

For his achievements in the field of science and education, Prof. Balarew has been repeatedly awarded prestigious Bulgarian and foreign awards, including: the honorary badge of the Bulgarian Academy of Sciences, the anniversary medal of the Chemical-Technical Institute-Burgas, the honorary medal "Acad. N.S. Kurnakov" of the Russian Academy of Sciences, the honorary medal of the University of Valladolid, Spain, the honorary badge (1st degree) of the Institute of General and Inorganic Chemistry-BAS, the honorary badge of BAS "Prof. Marin Drinov", a gold badge from the Federation of Scientific and Technical Unions in Bulgaria, the order "St. St. Cyril and Methodius" first degree, the order "St. St. Cyril and Methodius" with a necklace, the title "Honorary Citizen of Sofia", an honorary member of the Union of Chemists in Bulgaria.

The international chemical community celebrated the anniversary of Prof. Christo Balarew with a special article entitled "A Tribute to Christo Balarew" in the IUPAC journal *Chemistry International* and with a special issue of the *Journal of Solution Chemistry* dedicated to the jubilee. The Institute of General and Inorganic Chemistry of the Bulgarian Academy of Sciences celebrated on June 24, 2024 the ninetieth birthday of Prof. Balarew in the crowded hall "Prof. Marin Drinov" of BAS.

Be alive and healthy for many more years, Prof. Balarew! We wish you to realize a lot of new creative ideas!

Laboratory "Salt Systems and Natural Resources - IGIC – BAS

Bulgarian Chemical Communications, Volume 57, Issue 1 (pp. 7-13) 2025 *DOI: 10.34049/bcc.57.1.5578*

Kinetics of β-cyclodextrin production by cyclodextrin glucanotransferase from *Bacillus megaterium*

B. Y. Zhekova[1*], G. T. Dobrev[1], H. N. Panajotova[1], V. T. Dobreva[2], V. S. Stanchev[3]

[1]*Department of Biochemistry and Nutrition, University of Food Technologies, 26 Maritza Blvd., 4002 Plovdiv, Bulgaria*
[2]*Department of Engineering Ecology, University of Food Technologies, 26 Maritza Blvd., 4002 Plovdiv, Bulgaria*
[3]*Department of Automatics, Information and Control Systems, University of Food Technologies, 26 Maritza Blvd., 4002 Plovdiv, Bulgaria*

Received: May 19, 2023; Revised: January 07, 2025

The kinetics of β-cyclodextrin production by cyclodextrin glucanotransferase from *Bacillus megaterium* was investigated using two different approaches. By studying the initial rate of the enzyme reaction a strong inhibition of CGTase by the main product of the cyclization reaction β-CD was revealed. The type of inhibition was determined to be mixed competitive and uncompetitive. The value of the uncompetitive inhibition constant (K_{iu}=33.30 mg/mL) was much higher than the value of the competitive inhibition constant (K_{ic}=4.21 mg/mL), which indicated a predominance of the competitive part of the mixed type inhibition. The dynamics of β-CD formation and the corresponding starch degradation was investigated at real process conditions with different initial substrate concentrations. The enzyme reaction rate was maximal at the beginning of the process when the substrate current concentration was maximal. Depletion of the substrate led to a corresponding decrease in rate values. Another reason for the decrease in the enzyme rate was the accumulation of the product β-CD, which inhibited CGTase. The results for the dynamics of beta CD production were used for investigation of the kinetics of the process at real process conditions. In a real CD production process, CGTase showed a change in the type of inhibition by β-CD. The type of inhibition was determined to be competitive, with inhibition constant Ki=6.13 mg/mL. A probable reason for the change of the type of inhibition at real process conditions was the change in the substrate and product concentrations during the process.

Keywords: cyclodextrin glucanotransferase**,** cyclodextrins, enzyme kinetics, product inhibition, *Bacillus megaterium*

INTRODUCTION

Cyclodextrins (CD) are non-reducing cyclic oligosaccharides composed of 6, 7 or 8 α-1,4-linked glucose residues, denoted as α, β and γ, respectively. They are obtained under the catalytic action of cyclodextrin glucanotransferase (CGTase, EC 2.4.1.19). CGTase is a glycosyltransferase enzyme that displays four catalytic activities, named cyclization, coupling, disproportionation and hydrolysis [1, 2]. CD are formed by the cyclization activity of the enzyme. The cyclization activity of CGTase is an intramolecular transglycosylation reaction of long linear maltooligosaccharide chains, in which the cyclic ring structure of CD is formed [3]. CGTase can produce CD from substrates containing α-1,4-glycosyl chain, such as starch, dextrins, amylose, amylopectin, glycogen. The most widely used raw material for CD production is starch.

The processes for CD production described in the literature differ significantly in the yield of final products and the ratio between different CD types. The yield of CD varies from 15 to 93%, and the ratio α:β:γ - from the complete predominance of one type of CD to a mixture of all three types. Both the yield and the ratio of CD depend on the properties of CGTase, the type of substrate, its pre-treatment, the reaction conditions (substrate concentration, enzyme dosage, pH, temperature, duration of the process), the presence of organic compounds, etc. [4 – 7].

Despite of the selection of optimal reaction conditions, a complete conversion of the substrate to CD is not feasible. The main limiting factor is the product inhibition of CGTase by CD [8 – 11].

According to the literature, many CGTases are inhibited by the products of the cyclization reaction. The type of CD (α, β or γ) strongly inhibits the corresponding cyclization activity of the enzyme [12 –16]. Product inhibition of CGTase adversely affects the production of CD, as it leads to a reduction in the rate of product accumulation and/or to a complete cessation of the reaction, resulting in low CD yield.

Despite numerous reports of product inhibition of CGTase by CD, there are few explanations for this feature of the enzyme. According to Penninga *et al.* [17] CD bind to two parts of the enzyme molecule - the active site, which leads to competitive inhibition,

E-mail: zhekova_b@yahoo.com

and to the maltose-binding site in domain E, which disrupts its functions. Determination of the mechanism of inhibition is possible by studying the kinetics of the process. This also allows determination of the kinetic constants that have important technological meaning for the efficiency of the process.

Two approaches can be used to study product inhibition - experimental determination of the initial rate with the addition of different inhibitor concentrations [18] or determination of the rate during the process without additional introduction of inhibitor by studying the progress curves [19, 20]. The advantage of the second method is the obtaining of results that actually describe the process.

The aim of the present work is to study the kinetics of β-CD production by CGTase from *Bacillus megaterium* and to determine the type of inhibition and the values of the kinetic constants.

EXPERIMENTAL

CGTase enzyme preparation

Crude CGTase enzyme produced by *Bacillus megaterium* was used for the kinetics studies. The enzyme was a concentrate with an activity of 1.61E/mL. Enzyme production was described in a previous research [6, 21].

Determination of product inhibition of CGTase by β-CD

Product inhibition of CGTase by β-CD was studied by determination of the initial rate of the enzyme reaction at different concentrations of added inhibitor. Corn starch () was used as a substrate for cyclization reaction. The initial substrate concentration was in the range of 10-100 mg/mL, and the added product inhibitor β-CD varied in the range of 1-6 mg/mL. Corn starch suspensions with the desired concentrations were prepared in phosphate buffer with pH 7.0 by boiling in water bath for 10 min, the corresponding β-CD concentration and CGTase in the dosage of 2 U/g starch were added. The cyclization reaction was performed at 45°C for 10 min, the enzyme was inactivated by 10 min boiling and the concentration of β-CD formed was determined. The initial rate of the reaction was defined as the concentration of β-CD formed by the enzyme for 1 min under the assay conditions. The type of inhibition was determined by applying the Lineweaver–Burk transformation [18], and the kinetic constants K_m, V_m, and the inhibition constants K_{ic} and K_{iu} were calculated by using the model of mixed type inhibition:

$$v = \frac{V_m.S}{(K_m.(1+\frac{I}{Kic}) + S.(1+\frac{I}{Kiu}))} \quad (1)$$

v - initial rate of enzyme reaction, mg/(mL.min);

V_m – maximum rate of enzyme reaction, mg/(mL.min);

S – starch concentration, mg/mL;

K_m – Michaelis-Menten constant, mg/mL;

I – Inhibitor concentration, mg/ml;

K_{ic} – Competitive inhibition constant, mg/mL;

K_{iu} – Uncompetitive inhibition constant, mg/mL.

Investigation of the dynamics of β-CD production

The dynamics of β-CD production was studied at different corn starch () concentrations in the range of 10-100 mg/mL. Starch suspensions were prepared in phosphate buffer with pH 7.0 and heated in a boiling water bath for 10 min, cooled to 45°C and CGTase was added in a dosage of 2 U/g starch. The enzyme reaction was carried out at 45 °C with constant stirring for up to 7 h. Samples were taken at regular intervals, the enzyme was inactivated by boiling in a water bath for 10 min and the content of β-CD in the reaction mixture was determined.

Investigation of the kinetics of β-CD production by the progress curves of the process

The kinetics of the process of β-CD production was studied by the rate of product formation, defined as:

$$v = \frac{dP}{dt} \quad (2)$$

v – rate of enzyme reaction, mg/(mL.h);

P - concentration of β-CD, mg/mL;

t – time, h.

For determination of the type of inhibition and the kinetic constants reversible competitive and uncompetitive inhibition models were used [20]. The models for competitive and uncompetitive inhibition have the following type, respectively:

$$v = \frac{V_m.S}{K_m(1+\frac{I}{K_I}) + S} \quad (3)$$

$$v = \frac{V_m.S}{(K_m + S).(1+\frac{I}{K_I})} \quad (4)$$

v – rate of enzyme reaction, mg/(mL.h);

V_m – maximum rate of enzyme reaction, mg/(mL.h);

S – starch concentration, mg/mL;

K_m – Michaelis-Menten constant, mg/mL;

K_I – Inhibition constant, mg/mL.

The computing procedures were performed by using a package of applied software programs of own development in the software media of Matlab and Eureka [22]. The kinetic parameters for both models were calculated according to the optimization procedure minimizing the following criterion:

$$J = \sum_{i=1}^{n} (v_{\exp} - v_{\mathrm{mod}})^2 \rightarrow \min \qquad (5)$$

v_{exp} – experimental values of enzyme reaction rate, mg/(mL.h);

v_{mod} – predicted values of enzyme reaction rate, mg/(mL.h);

n – number of analyzed points.

Assays

The concentration of β-CD was determined by the spectrophotometric method with phenolphthalein. A freshly prepared solution of 1 part of 3.8 mM phenolphthalein in 95 % ethanol and 50 parts of carbonate buffer (pH=10.5) was prepared. Appropriately diluted samples of the reaction mixture were mixed with 2.0 mL of the phenolphthalein solution and distilled water to a final volume of 5.0 mL. The absorbance was measured at 550 nm against a blank sample, containing a mixture of water and phenolphthalein. β-Cyclodextrin concentration was calculated using a calibration curve. Starch concentration was determined by the method described by Thiemann *et al.* [23].

RESULTS AND DISCUSSION

Product inhibition of CGTase by β-CD

Most known CGTases are reported to be characterized with strong product inhibition by the predominant type of CD [12 – 14]. The investigated CGTase produced the three types of CD, and the predominant type was β-CD independently of the reaction conditions [11]. In order to determine the type of inhibition of the enzyme by β-CD, the kinetics of the process was studied. The initial rate of β-CD formation (v) was investigated at starch concentrations (S) in the range of 10-100 mg/mL with addition of 1-6 mg/mL inhibitor β-CD. The results are plotted in accordance with Lineweaver–Burk transformation in Fig. 1.

The results confirmed that CGTase from *B. megaterium* was strongly inhibited by the main product of the cyclization reaction. The studying of the Lineweaver–Burk plot (Fig. 1.) revealed a mixed type of inhibition of CGTase by β-CD. In the presence of β-CD both kinetic constants K_m and V_m were changing, and the inhibition was actually combined competitive and uncompetitive.

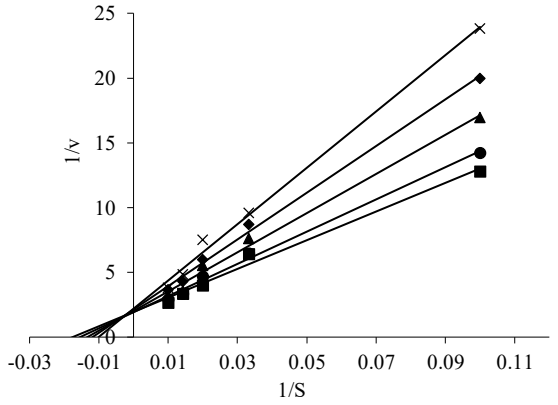

Fig. 1. Lineweaver–Burk plot of product inhibition of CGTase by different concentrations of β-CD: ■ 1 mg/mL, ● 2 mg/mL ▲ 3 mg/mL ◆ 5 mg/mL × 6 mg/mL.

The values of the kinetic and inhibition constants for mixed type inhibition in the presence of β-CD were calculated (Table 1). It was noted that the value of the uncompetitive inhibition constant (K_{iu}) was much higher than the value of the competitive inhibition constant (K_{ic}). This indicated a predominance of the competitive part of the mixed type inhibition. A mixed type of inhibition was also proved for other CGTases predominantly producing β-CD [12], while competitive inhibition was observed for enzymes forming mainly α-CD [12, 24].

Table 1. Kinetic and inhibition constants of CGTase for mixed type inhibition by β-CD

K_m, mg/mL	V_m, mg/(mL.min)	K_{ic}, mg/mL	K_{iu}, mg/mL
46.93	0.54	4.21	33.30

Dynamics of β-CD formation

The established mixed type of product inhibition by β-CD is an important characteristic of CGTase but it refers to the initial rate of the enzyme reaction at certain reaction conditions. It does not actually describe the process of β-CD production, which can be performed at different reaction conditions, with long duration of the process and at different actual concentrations of the product inhibitor. In order to study the product inhibition of CGTase by β-CD at real process conditions, the dynamics of β-CD formation and starch degradation were investigated at five different initial substrate concentrations. The results are presented in Fig. 2 A-E.

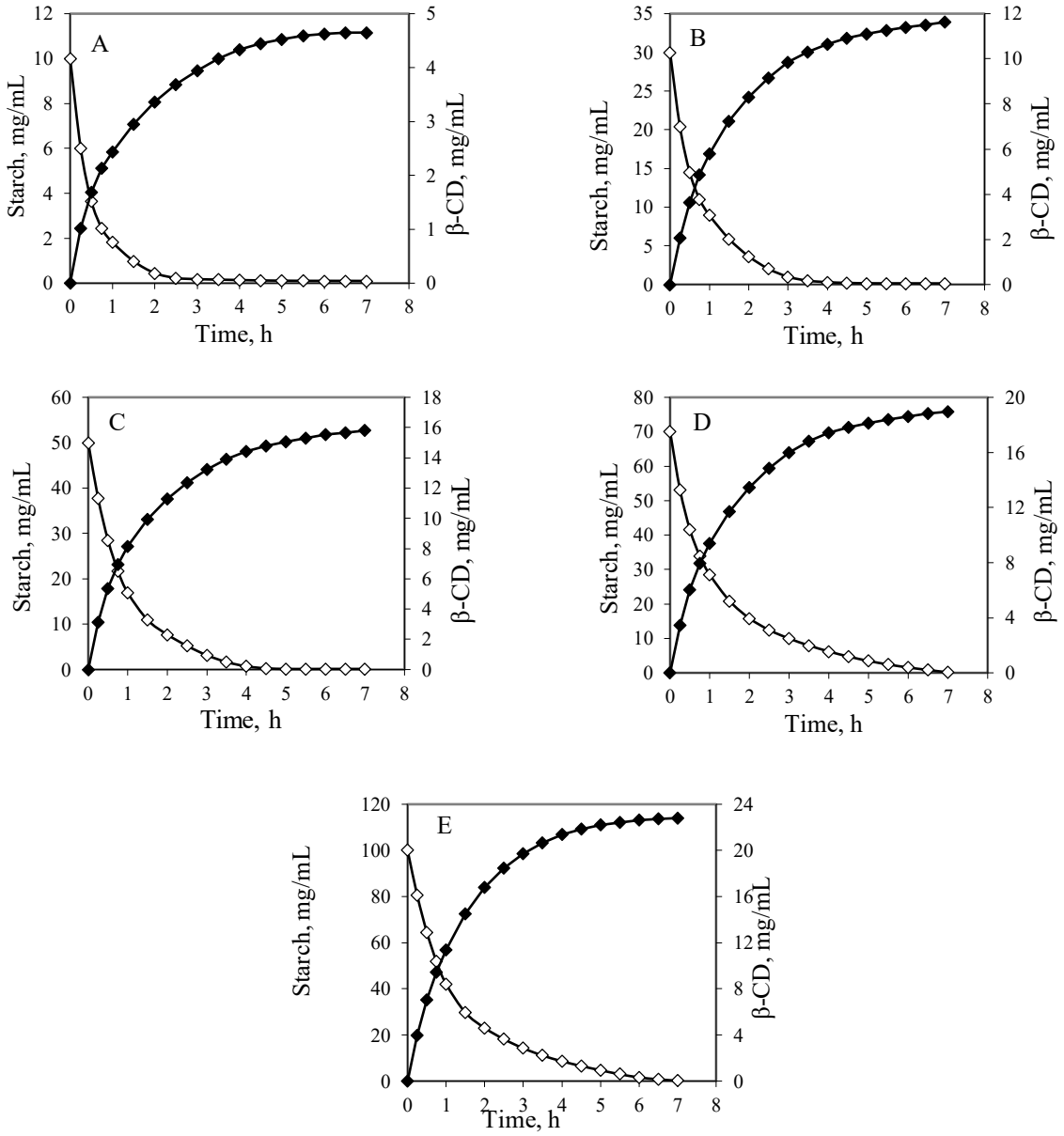

Fig. 2. Dynamics of β-CD formation (◆ β-CD) and starch degradation (◇ Starch) at different initial starch concentrations: A-10 mg/mL starch; B-30 mg/mL starch; C-50 mg/mL starch; D-70 mg/mL starch; E-100 mg/mL starch

For all studied initial substrate concentrations, the enzyme reaction started at high speed. The main amount of product was accumulated in the first 4 hours of the process. The rapid formation of β-CD corresponded to the rapid degradation of the substrate. At a starch concentration of 50 mg/mL, 50 % of the available substrate was depleted in the first 30 min.

The higher starch concentration required longer enzyme action. In this case, however, a reaction time of 5 hours was sufficient to form most of the product and thus to degrade most part of the substrate.

Kinetics of β-CD production by the progress curves of the process

In Fig. 3 the calculated rate values of the enzyme reaction are presented as a function of the current substrate concentration during the process. The results for the respective product concentration are also included.

The enzyme reaction rate was maximal at the beginning of the process when the substrate current concentration was maximal. The highest rate was reached at 100 mg/mL of starch. Depletion of the substrate led to a corresponding decrease in rate values. When comparing the results of Fig. 3 A-E it

was clear that substrate depletion was not the only reason for rate reduction. Provided the same amount of starch, the reaction rate depended on the concentration of β-CD in the reaction medium. This is illustrated in Fig. 4, where the rate of the process is represented as a function of the concentration of β-CD at the same current starch concentration.

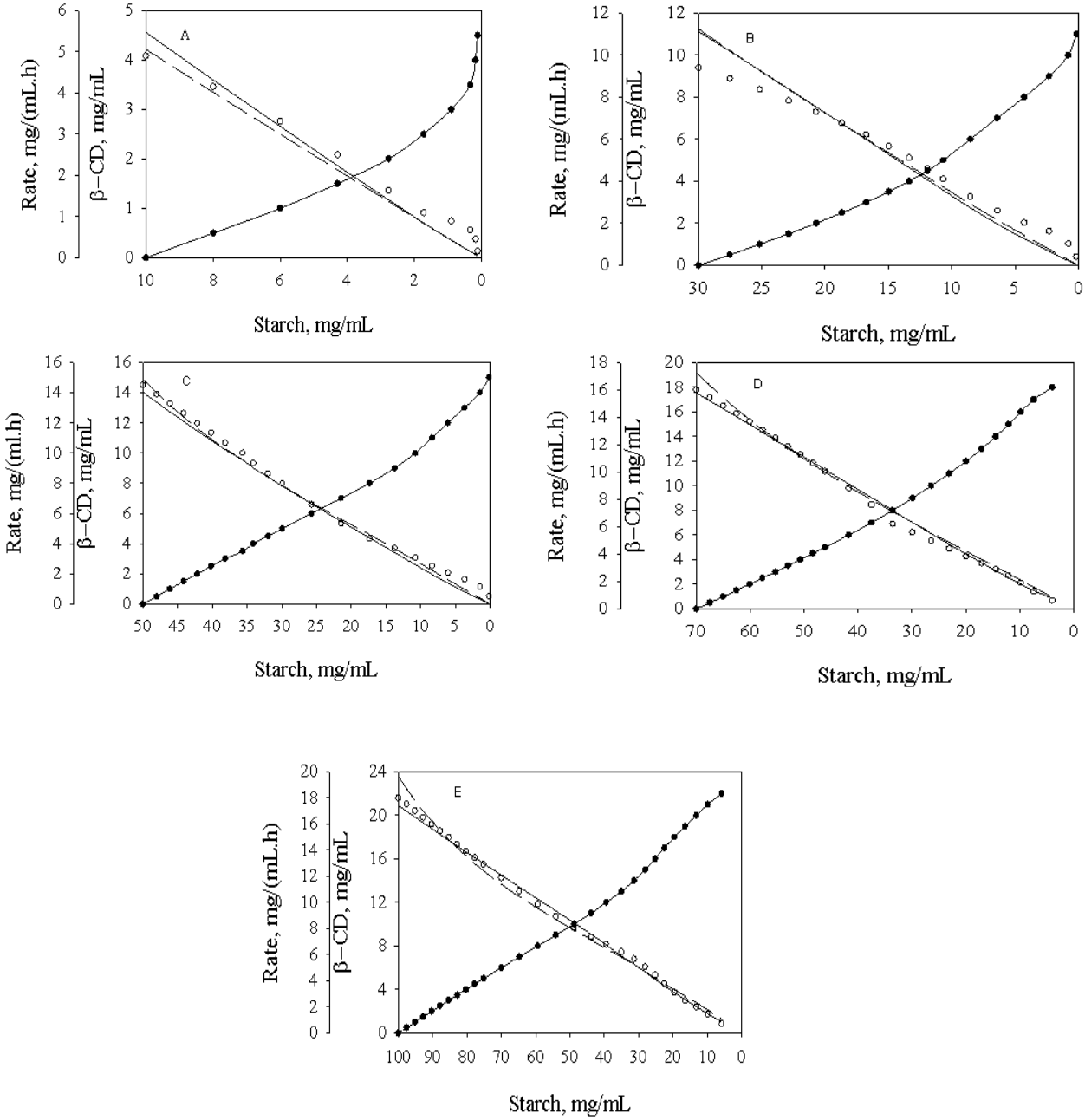

Fig. 3. Dependence of the enzyme reaction rate on current substrate concentration: ● experimental β-CD values; ○ experimental enzyme reaction rate; ─ model values for competitive inhibition; - - model values for uncompetitive inhibition at different initial starch concentrations: A-10 mg/mL starch; B-30 mg/mL starch; C-50 mg/mL starch; D-70 mg/mL starch; E-100 mg/mL starch.

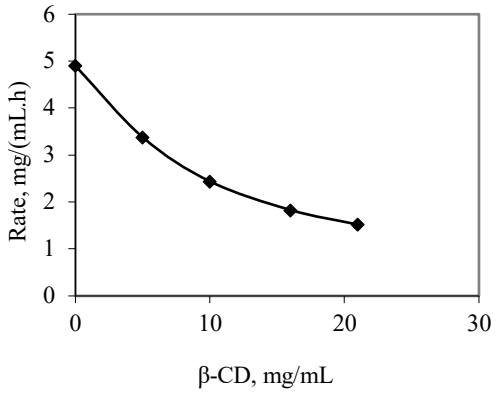

Fig. 4. Inhibition of CGTase by β-CD at current starch concentration of 10 mg/mL

The results showed that the increase in the concentration of the product led to a significant decrease in enzyme reaction rate. Even in the presence of only 5 mg/mL of β-CD, the process rate decreased by about 30%, and at 10 mg/mL CGTase synthesized β-CD at a twice lower rate. This fact is an indication of the strong effect of β-CD concentration on β-CD production process and it is in accordance with the established product inhibition of CGTase.

In order to determine the type of inhibition of the β-CD production process in real process conditions, the results of Fig. 3 A-E were processed according to models for mixed type (1), competitive (3) and uncompetitive inhibition (4). Though CGTase showed mixed type inhibition by β-CD by studying the initial rate of the enzyme reaction, this was not proved for real process conditions. The experimental data did not fit the model for mixed type inhibition (data not shown). For these reasons models for competitive (3) and uncompetitive inhibition (4) were evaluated. The calculated model values of rate and product concentration by the two models studied are presented in Fig. 3 A-E with lines. The variance of the models from the experimental values was used to evaluate the obtained models. The values of the kinetic parameters determined by equations (3) and (4) are presented in Table 2.

Table 2. Kinetic and inhibition constants of β-CD production

Constants	Competitive inhibition	Uncompetitive inhibition
V_m, mg/(mL.h)	23.01	29.03
K_m, mg/mL	32.02	47.43
K_i, mg/mL	6.13	11.53

The competitive inhibition model better described the process of β-CD production. This result is explainable given the mechanism of action of CGTase. β-CD compete with starch for a place in the active site and under appropriate conditions CGTase exhibits decyclization activity. The larger deviations of the models from the experimental results are observed at low initial starch concentration (Fig. 3 A, B). We hypothesize that this was due to the low concentration of β-CD and the limitation by substrate.

CONCLUSIONS

CGTase from *B. megaterium* was strongly inhibited by the main product of the cyclization reaction β-CD. By studying the initial rate of the enzyme reaction the type of inhibition was proved to be combined competitive and uncompetitive. The value of the uncompetitive inhibition constant (K_{iu}=33.30 mg/mL) was much higher than the value of the competitive inhibition constant (K_{ic}=4.21 mg/mL). This indicated a predominance of the competitive part of the mixed type inhibition.

At real process conditions, CGTase did not show a mixed type inhibition by β-CD. The process of β-CD production was influenced by competitive inhibition of the enzyme by β-CD, with inhibition constant Ki=6.13 mg/mL. A probable reason for the change of the type of inhibition at real process conditions was that the concentration of the product increased during the process and reached values much higher than the values available at the initial reaction time. At the same time, at long durations of the process, the substrate was depleted and reached minimal levels. This obviously led to a change of the type of inhibition from mixed to competitive, as beta CD compete with the substrate for the active sites of the enzyme.

REFERENCES

1. K. Saini, V. M. Pathak, A. Tyagi, R. Gupta, *Catal. Res.*, **2**, 029 (2022).
2. B. A. Van Der Veen, J. C. M. Uitdehaag, D. Penninga, G. J. W. M. Van Alebeek, L. M. Smith, B. W. Dijkstra, L. Dijkhuizen, *J. Mol. Biol.*, **296,** 1027 (2000).
3. C. H. Lim, B. Rasti, J. Sulistyo, M. A. Hamida, *Heliyon*, **7,** e06305 (2021).
4. H. F. Alves-Prado, A. A. J. Carneiro, F. C. Pavezzi, E. Gomes, M. Boscolo, C. M. L. Franco, R. da Silva, *Appl. Biochem. Biotechnol.*, **146**, 3 (2008).
5. G. Matioli, G. Zanin, F. De Moraes, *Appl. Biochem. Biotechnol.,* **91-93**, 643 (2001).
6. I. Pishtiyski, B. Zhekova, *World J. Microbiol. Biotechnol.*, **22**, 109 (2006).
7. A. M. M. Sakinah, A. F. Ismail, O. Hassan, A. W. Zularisam, R. Md. Illias, *Desalination*, **239**, 317 (2009).
8. M. B. Arce-Vázquez, E. Ponce-Alquicira, E. Delgado-Fornué, R. Pedroza-Islas, G. Díaz-

Godínez, J. Soriano-Santos, *Front. Microbiol.*, **7**, 1513 (2016).
9. S. Chen, Z. Li, Z. Gu, Y. Hong, L. Cheng, C. Li, *Int. J. Biol. Macromol.*, **136**, 460 (2019).
10. L. N. Koga, V. C. Fenelon, J. H. Miyoshi, C. Moriwaki, K. B. B. Wessel, C. S. Mangolim, G. Matioli, *Braz. J. Pharm. Sci.*, **56**, e18993 (2020).
11. B. Zhekova, I. Pishtiyski, V. Stanchev, *Food Technol. Biotechnol.*, **46,** 328 (2008).
12. C. Li, Q. Xu, Z. Gu, S. Chen, J. Wu, Y. Hong, L. Cheng, Z. Li, *J. Mol. Catal. B: Enzym.*, **133**, 203 (2016).
13. B. Gawande, A. Patkar, *Starch/Stärke* **53**, 75 (2001).
14. K. Tomita, T. Tanaka, Y. Fujita, K. Nakanishi, *J. Ferment. Bioeng.,* **70**, 190 (1990).
15. T. Kim Y. Lee, H. Kim, *Biotechnol. Bioeng.*, **39**, 977 (1992).
16. Y. Lee, H. Kim, *Biotechnol. Bioeng.*, **39**, 977 (1992).
17. D. Penninga, B. Van der Veen, R. Knegtel, H. Rozeboom, K. Kalk, L. Dijkuizen, B. Dijkstra, *The J. Biol. Chem.*, **271,** 32777 (1996).
18. A. Cornish-Bowden, Fundamentals of enzyme kinetics, Portland Press, London, 1995.
19. M. Desouza, S. H. B. Faria, G. M. Zanin, F. F. Moraes, *Chem. Eng. Trans.*, **32**, 1111 (2013).
20. A.G. Marangoni, Enzyme kinetics a modern approach, John Wiley & Sons, Inc. Hoboken, New Jersey, 2003.
21. V. Popova, I. Pishtiyski, *Eur. Food Res. Technol*., **213**, 67 (2001).
22. I. Stoilova, A. Krastanov, V. Stanchev, *Adv. Biosci. Biotechnol.*, **1**, 208 (2010).
23. V. Thiemann, C. Dönges, S. Prowe, R. Sterner, G. Antranikian, *Archiv. Microbiol.*, **182**, 226 (2004).
24. H. Leemhuis, B. W. Dijkstra, L. Dijkhuizen, *Eur. J. Biochem*., **270**, 155 (2003).

Bulgarian Chemical Communications, Volume 57, Issue 1 (pp. 14-19) 2025 *DOI: 10.34049/bcc.57.1.5609*

Extraction of cellulose from rice straw by microwave irradiation

N. O. Appazov[1,2]*, I. D. Espanova[1], D. Zh. Niyazova[1], A. A. Moldanazar[1], R. U. Zhapparbergenov[1,3], R. A. Turmanov[1,4], A. B. Toibazarova[1], A. N. Appaz[5], M. I. Syzdykbayev[1]

[1]*Korkyt Ata Kyzylorda University, 29A Ayteke bi Str., Kyzylorda, Republic of Kazakhstan*
[2]*Limited Liability Partnership «CNEC», Dariger Ali Str., Kyzylorda, Republic of Kazakhstan*
[3]*Limited Liability Partnership «KazEcoChem», 12 D. Konaev Str., Astana, Republic of Kazakhstan*
[4]*Limited Liability Partnership «DPS-Kyzylorda», 112A Amangeldi Str., Kyzylorda, Republic of Kazakhstan*
[5]*Nazarbayev Intellectual School Chemical-Biological Direction in Kyzylorda, 6 Sultan Beybars Str., Kyzylorda, Republic of Kazakhstan*

Received: October 01, 2023; Revised: August 17, 2024

This article examines the process of converting large volumes of agricultural waste - rice straw - into cellulose which can be used for paper products manufacturing. The process of rice straw delignification is carried out using microwave irradiation at power levels of 100 and 180 W for 5-40 min with a sodium hydroxide solution. The delignification of the obtained product is also performed under microwave irradiation at power levels of 100 and 180 W for 5-40 min, using a mixture of acetic acid and hydrogen peroxide at a 1:1 ratio in the presence of ammonium molybdate (0-5 wt.% of cellulose mass). Concentrated sodium hypochlorite solution is used for bleaching of the obtained mass. The yield of the target product, cellulose, is 42.7-70.3 wt.%. The optimal product is cellulose obtained after delignification using a mixture of acetic acid and hydrogen peroxide in a 1:1 ratio under microwave irradiation with a power of 180 W for 15 min in the presence of ammonium molybdate (5% of the cellulose mass) and without using sodium hypochlorite. In this case, the content of alpha-cellulose in the final product is 74.45 wt.%, corresponding to Grade A2 (cellulose used for the production of white office paper). The obtained results have potential application in paper products manufacturing.

Keywords: rice straw, cellulose, microwave irradiation, paper products

INTRODUCTION

Cellulose, also known as plant fiber, is the main component of plant cell walls and, combined with other substances (incrustants), forms the structural framework of all plant organisms. In its purest form, cellulose is found, for example, in cotton fibers (up to 96-98%). Wood contains not only cellulose but also hemicellulose, lignin, resins, fats, proteins, and dyes. Dry wood contains about 40-60% alpha-cellulose, that is, cellulose insoluble in a 17.5-18% solution of alkali at room temperature [1]. To obtain high-quality cellulose, a bleaching process is crucial. Most factories use chlorine bleaching for this purpose, which allows obtaining highly purified cellulose. This method is used, for example, for producing kraft pulp and other grades [2]. Cellulose finds applications in various industries, such as pharmaceuticals (as an auxiliary substance in the production of medicinal products, suspensions, ointments, creams) [3], cosmetics (for creating creams, powders, suspensions, and other cosmetic products), food industry (in the production of mayonnaise, pastes, creams, canned meat, fish, dairy products, etc.), chemical industry (as raw material for further processing, including obtaining nanocrystalline cellulose, nanocomposites, ethers, copolymers), road coverings (to improve asphalt characteristics), and many other areas [4-7]. Rice is one of the key agricultural crops globally, providing sustenance for nearly half of the world's population. Its importance in production remains constant for both current and future food security concerns. In parallel with population growth, the demand for rice continues to increase, particularly in Asia and Africa [8]. However, the cultivation of rice poses various ecological challenges, such as the pollution caused by burning rice straw residues in fields. This issue is particularly complex and presents a significant challenge for technical experts in these regions. Nevertheless, numerous alternatives to burning straw are being explored, and research is being conducted to assess ways to reduce the environmental impact of rice production.

In recent times, various methods for converting rice waste into valuable products have been proposed. Our team has previously conducted work

* To whom all correspondence should be sent:
E-mail: *nurasar.82@mail.ru*

on transforming rice waste into a promising fertilizer - biochar, and a widely applicable adsorbent - activated carbon [9-12].

In this study, we propose the processing of rice straw into cellulose by carrying out processes of desiliconation with sodium hydroxide solution, and delignification with a mixture of acetic acid and hydrogen peroxide under microwave irradiation. Microwave activation of many organic processes is a rapidly developing field, allowing process durations to be reduced by orders of magnitude [13].

MATERIALS AND METHODS OF RESEARCH

To obtain cellulose from rice straw, the latter was initially crushed using a DKU-05 grinder (Russia). Then the crushed mass was washed with water and dried at a temperature of 25°C. Subsequently, 10 g of the crushed, washed, and dried rice straw were placed into a glass container, and 130 ml of sodium hydroxide solution with a concentration of 0.1 mol/L was added. The delignification process was conducted by irradiating the mixture with microwave beams at power levels of 100 and 180 W for 5-40 min. After irradiation, the decalcified cellulose mass was cooled to a temperature of 25°C, washed with distilled water until neutral pH, and then dried at 25°C. The resulting product was subjected to a delignification process, wherein 130 ml of a mixture of icy acetic acid and 37% hydrogen peroxide in a 1:1 ratio, along with ammonium molybdate (0-5% of the dry decalcified cellulose mass), was irradiated with microwave beams at power levels of 100 and 180 W for 5-40 min. Subsequently, the cellulose mass was washed until neutral pH. A saturated solution of sodium hypochlorite was added to the purified dry mass for bleaching (in some cases no bleaching was required). The yield of the final product ranged from 42.7% to 70.3%. The content of alpha-cellulose was determined by treating the obtained cellulose with a 17.5% sodium hydroxide solution (purged of carbonates) for 30 min followed by washing with distilled water and treatment with a 10% acetic acid solution for 30 min. After treatment, the cellulose was washed with distilled water and dried at a temperature of 105-135°C until a constant mass was achieved. The obtained mass was then weighed using analytical scales to determine the yield of alpha-cellulose [14]. IR spectra were taken on an IR-Prestige 21 instrument of Shimadzu (Japan, 2008) in the wavelength range 400-4000 cm^{-1} without special preparation of the sample on the DuraSamplIR II attenuated total reflection (ATR) module with a single reflection (prism material is diamond on ZnSe substrate) of Smiths (USA). To study the surface morphology of cellulose samples, SEM analysis was performed, and microphotographs were taken on a JSM-6510 LV device manufactured by Jeol (Japan). Measurements were carried out in high vacuum mode using a secondary electron detector at an accelerating voltage of 25 kV. The crystal structure of MCC was studied by X-ray diffraction on an X´PertPRO diffractometer (Malvern Panalytical Empyrean, Netherlands) using monochromatized copper (CuKα) radiation with a scan step of 0.02°, K-Alpha1 [Å] 0.1542. The measurement angle was 10-40°, the X-ray tube voltage was 40 kV, the current intensity was 30 mA, the measurement time at each step was 0.5 s and an aluminum rectangular multi-purpose sample holder (PW1172/01) was used for the measurement in reflection mode.

RESULTS AND DISCUSSION

Various methods for producing cellulose are known, involving the use of cereal straw, cane crops or oilseeds, for example wheat straw, sunflower husks. In these methods, the straw is subjected to autohydrolysis at 180-220°C, pressures of 10-20 atm, and durations of 5-15 min, followed by pressure release. The autohydrolyzed mass is then twice extracted with dilute 0.4-1% NaOH solution or an organic lignin solvent (such as acetone, dioxane, ethyl alcohol, etc.). Subsequently, the mass is washed with distilled water and treated with a standard hydrogen peroxide bleach solution, followed by washing and drying at a temperature of 25°C. As the aqueous extract contains primarily autohydrolyzed sugars, it can be of significant interest for yeast production or as animal feed additive [15-17].

However, these methods have drawbacks, including technological complexity, use of specific autoclave equipment, elevated pressure, high temperature, and prolonged duration.

This study provides data on the extraction of cellulose from rice straw using microwave irradiation. Delignification is carried out using a 4 wt.% potassium hydroxide solution for 10-40 min at an irradiation power of 480 W. Subsequently, the material is treated with a 2.5 wt.% hydrogen peroxide solution and left for one night, followed by irradiation for 10 min at 480 W. Afterward, the material is washed with water until neutral pH and then dried under vacuum. Acidic treatment with acetic acid is conducted for 10-40 min at an irradiation power of 480 W. The material is then centrifuged, washed with water, and dried at a temperature of 25°C. Depending on the conditions, the product yield ranges from 48.6% to 67.3% [18]. Drawbacks of this approach include the use of the

more expensive potassium hydroxide instead of sodium hydroxide, higher power levels of microwave irradiation, extended process duration, and relatively low product yield.

The present study addresses these drawbacks by irradiating the material with microwave beams at power levels of 100-180 W for 5-40 min, using a 1:1 ratio of icy acetic acid and 37% hydrogen peroxide (10% and 50% aqueous solution, respectively), applying ammonium molybdate as a catalyst (0.1%, 1%, and 5%), and sodium hypochlorite for bleaching (in some cases, the use of a mixture of hydrogen peroxide and acetic acid did not give the required whiteness, therefore a 10% sodium hypochlorite solution was used).

To determine the optimal conditions for obtaining cellulose from rice straw, a series of experiments were conducted, as detailed in the table.

The obtained products were analyzed for alpha-cellulose content according to the method [14]. Based on the results of the experimental investigations, the products obtained under the conditions specified in items 12, 13, and 15 of the table correspond to Grade A2 cellulose, which is used for the production of white office and laboratory filter paper. The products obtained according to items 14 and 16 correspond to Grade B2 cellulose, used for manufacturing paper napkins, towels, school notebooks, toilet and laboratory filter paper. The products obtained according to items 1-11 and 17-23 correspond to unbleached cellulose, used for producing wrapping (kraft) paper and cardboard products [19].

A photograph of the obtained products, as specified in the table, is provided in Figure 1.

Table Determination of optimal conditions for cellulose extraction from rice straw under microwave irradiation

№	Microwave radiation power, (W)	Duration, (min)	Catalyst, (%)	Sodium hypochlorite, (ml)	Ratio of acetic acid to hydrogen peroxide (H_2O_2)	Yield of the target product, (%)
1	100	5	5	100	1:1	70.30
2	100	10	5	100	1:1	61.01
3	100	15	5	100	1:1	61.32
4	100	20	5	100	1:1	57.26
5	100	25	5	100	1:1	50.98
6	100	30	5	100	1:1	54.68
7	100	30	5	no chlorine	1:1	59.66
8	100	35	5	100	1:1	53.53
9	100	40	5	100	1:1	57.51
10	180	5	5	100	1:1	61.77
11	180	10	5	100	1:1	57.22
12	180	15	5	-	1:1	46.01
13	180	20	5	-	1:1	46.05
14	180	15	1	-	1:1	47.06
15	180	15	0,1	-	1:1	47.95
16	180	15	-	-	1:1	42.77
17	180	15	-	100	10% aqueous solution of mixture	62.62
18	180	15	-	-	50% aqueous solution of mixture	62.89
19	180	15	-	100	50% aqueous solution of mixture	59.59
20	180	20	-	-	50% aqueous solution of mixture	62.79
21	180	20	-	100	50% aqueous solution of mixture	51.59
22	180	25	-	-	50% aqueous solution of mixture	68.96
23	180	25	-	100	50% aqueous solution of mixture	51.48

Figure 1. Photograph of the obtained products according to the table

The cellulose obtained according to item 12 of the table exhibited notable whiteness. Due to this, an analysis was conducted on this product to determine its alpha-cellulose content in accordance with the methodology [14]. The alpha-cellulose content in this product was measured to be 74.75%, which corresponds to Grade A2 cellulose.

The IR spectrum shows absorption bands at 663 cm^{-1} (C-OH bonds), 898 cm^{-1} and 1157 cm^{-1} (glycosidic C-O-C), an intense band at 1029 cm^{-1} (pyranose C-O), 1226 cm^{-1} and 1319 cm^{-1} C-H bond vibrations, 1431 cm^{-1} vibrations of CH_2, 1647 - OH due to water molecules sorbed from air, 2846 absorption band of CH-, broad absorption band of associated -OH group in the region of 3000-3500 cm^{-1} (Figure 2).

The surface morphology of the cellulose obtained from rice straw is shown in Figure 3. The cellulose fibers are 3-5 μm wide and the surface is clean and relatively smooth.

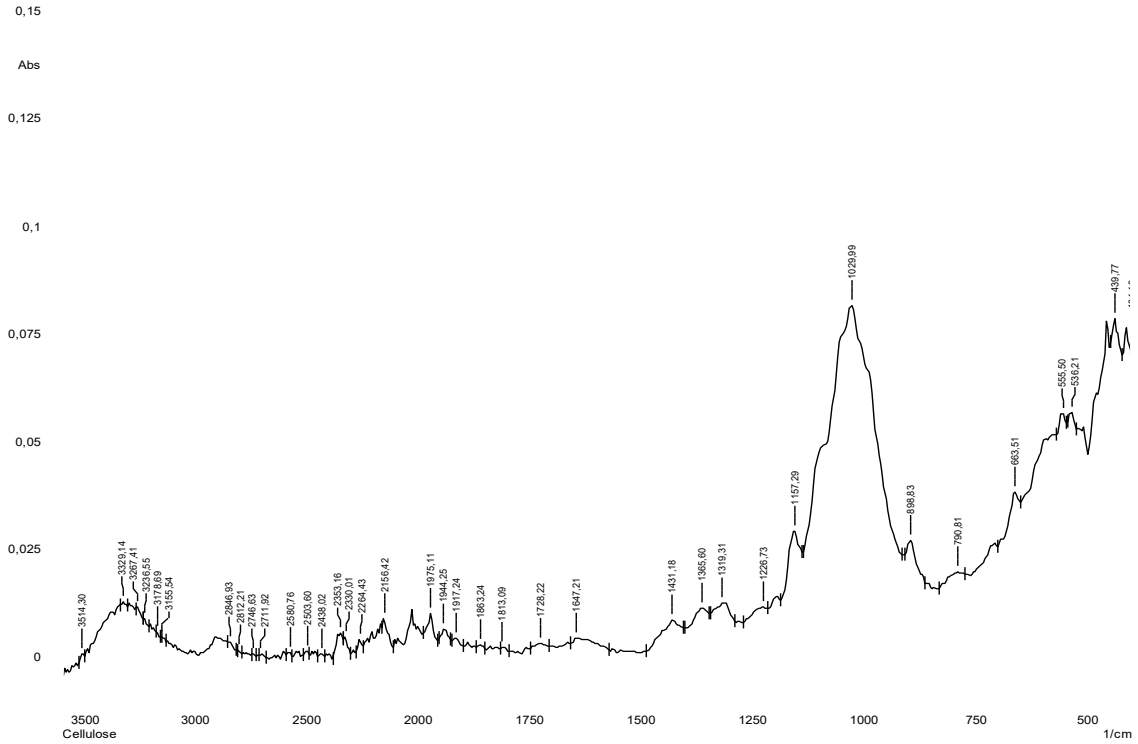

Figure 2. IR spectrum of cellulose obtained from rice straw under optimal conditions

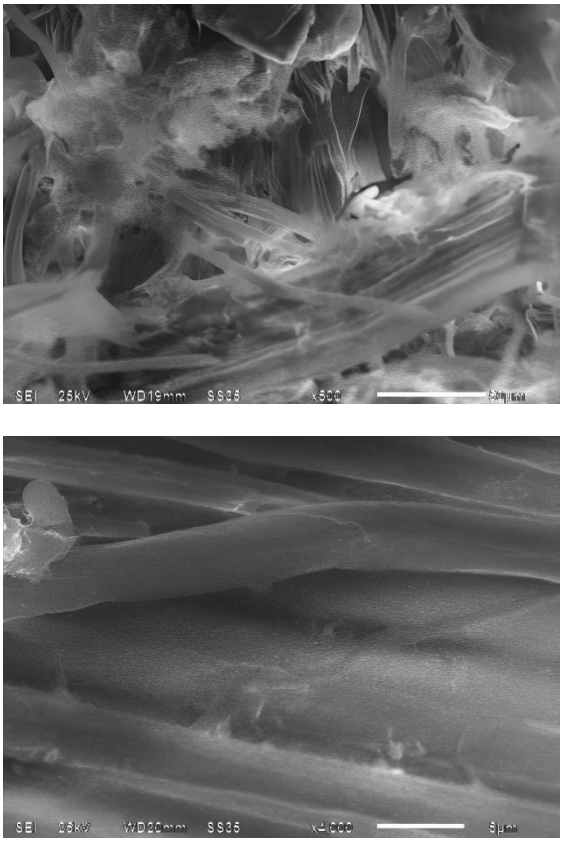

Figure 3. SEM image of cellulose obtained from rice straw under optimal conditions

On the X-ray diffraction pattern of the obtained MCC in Figure 2 three diffraction peaks were registered. They are equal to $2\theta=15.5^0$, 21.7^0, 34.7^0 and the crystal structure of the molecule is double-stranded monoclinic, cellulose I β showed diffraction peaks [17, 20]. The crystal structure of the MCC obtained in the refs. [21, 22] is consistent with the results of the present study. This indicates that the crystal structure of the material obtained in this investigation is typical for MCC (Figure 4).

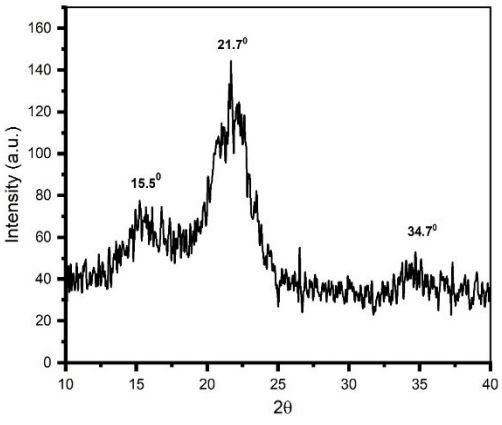

Figure 4. X-ray diffraction pattern of cellulose obtained from rice straw under optimal conditions

CONCLUSION

The proposed method for obtaining cellulose from rice straw offers several advantages compared to known methods:

- It utilizes agricultural waste in the form of rice straw;
- The use of microwave irradiation enhances energy efficiency;
- The process duration is significantly reduced;
- The sodium hydroxide concentration required for delignification is lowered;
- High pressure is eliminated from the delignification process;
- The catalyst quantity in the delignification process is reduced or eliminated;
- Reduced amounts of hydrogen peroxide and acetic acid are used in the delignification process.

The results of the experimental research not only facilitate the rational utilization of natural resources but also hold environmental significance. Furthermore, the approach aligns with the principles of green chemistry.

Funding: *This study was supported by PhytoAPP EU framework (2021-2025). The PhytoAPP project has received funding from the European Union's HORIZON 2020 research and innovation programme under the Marie Sklodowska-Curie grant agreement 101007642. This publication reflects only the authors' views and the European Commission is not liable for any use that may be made of the information contained therein.*

REFERENCES

1. I. P. Muhlenov, A. Ja. Averbuh, D. A. Kuznecov, A. G. Amelin, E. S. Tumarkina, I.J e. Furmer, Obshhaja himicheskaja tehnologija, Vysshaja shkola, Moscow, 1977. (in Russian)
2. G. L. Koren'kov, A. G. Dedov, N. A. Ustinova, I. L. Safonova, N. N. Romashova, T. M. Najshuler, G. G. Afanas'eva, A. S. Morozova, A. A. Cherkasova, Himicheskaja promyshlennost' SShA, Nauchno-issledovatel'skij institut tehniko-jekonomicheskih issledovanij, Moscow, 1972. (in Russian).
3. T. A. Sokol'skaja. *Himiko-farmacevticheskij Zhurnal*, **10**, 22 (2010), (in Russian).
4. H. X. Bian, Y. Y. Yang, P. Tu, J. Y. Chen, *Membranes*, **12**(5), 17 (2022).
5. Z. X. Li, T. T. Guo, Y. Z. Chen, J. Y. Liu, J. Y. Ma, J. Wang, L. H. Jin, *Materials Research Express*, **9**(2), 16 (2022).
6. A. Sharma, T. Mandal, S. Goswami, *Trends in Carbohydrate Research*, **9** (4), 16 (2017).
7. G. A. Petropavlovskij, N. E. Kotel'nikova, Mikrokristallicheskaja celljuloza (obzor), Himija drevesiny, 1976, (in Russian).
8. A.N.M.R. Bin Rahman, J.H. Zhang. *Food and Energy Security*, **12**(2), (2023).
9. N. O. Appazov, B. M. Bazarbayev, T. Assylbekkyzy, B. M. Diyarova, S. A. Kanzhar, S. Magauiya, R. U. Zhapparbergenov, N. I. Akylbekov, B. A. Duisembekov, *News of the Academy of Sciences of the Republic of Kazakhstan*, **1** (445), 66 (2021).
10. B. Diyarova, N. Appazov, B. M. Bazarbayev, B. Dzhiembaev, O. Lygina, A. S. Tapalova, *Egyptian Journal of Chemistry*, **66** (SI-13), 1871 (2023).
11. G. Yergaziyeva, M. Mambetova, N. Makayeva, B. Diyarova, N. Appazov, *Journal of Composites Science*, **8,** 376 (2024).
12. L. I. Akhmetov, I. F. Puntus, R. A. Narmanova, N. O. Appazov, T. V. Funtikova, A. A. Regepova, A. E. Filonov. *Processes,* **10**, 549 (2022).
13. S. S. Berdonosov, *Soros Educational Journal*, **7(1)**, 32 (2001).
14. GOST 595-79. Celljuloza hlopkovaja. Tehnicheskie uslovija. Data vvedenija 01.07.1980. Izdanie 08.2002 s izmenenijami, M., Izdatel'stvo standartov, 2002 (in Russian).
15. Ju. K. Jakobsons, P .P. Jerin'sh, A. Ja. Kul'kevic, A. G. Polmanis, *USSR Patent* 1792942 (1993).
16. A. A. Sejtmagzimov, G. M. Sejtmagzimova, A. Saipov, M. I. Sataev, Ju. V. Sevast'janova, *Kazakhstan Patent* 31671, (2016).
17. K. Akatan, S. Kabdrakhmanova, T. Kuanyshbekov, Z. Ibraeva, A. Battalova, K. S. Joshy, S. Thomas, *Cellulose,* **29**, 3787 (2022).
18. G. Z. Fan, Y. X. Wang, G. S. Song, J. T. Yan, J. F. Li, *Journal of Applied Polymer Science,* **134** (22), 8 (2017).
19. GOST 9094-89. Bumaga dlya pechati ofsetnaya. Data vvedeniya 22.06.1989. Gosudarstvennyj komitet SSSR po standartam, Moskva, 1989 (in Russian).
20. J. Trifol Guzman, C. Sillard, D. Plackett, P. Szabo, J. Bras, A. E. Daugaard, *Cellulose,* **24(1)**, 107 (2017).
21. A. A. Imasheva, S. K. Kabdrakhmanova, J. E. Ibraeva, S. E. Kudai, **1(81)**, 35 (2020) (in Kazakh).
22. A. K. Battalova, S. K. Kabdrakhmanova, K. Akatan, M. M. Beisebekov, N. Kantay, Zh. E. Ibraeva, A. M. Mausumbayeva, L. Merck, *International Journal of Biology and Chemistry* **16 (1)**, 78 (2023).

Bulgarian Chemical Communications, Volume 57, Issue 1 (pp. 20-25) 2025 *DOI: 10.34049/bcc.57.1.5630*

Textural properties of sweet pepper depending on genotype and method of cultivation

N. Đinović[1], G. Pevicharova[2]*, V. Slavova[2]

[1] *Superior D.O.O, Velika Plana, Republic of Serbia*
[2] *Laboratory for Vegetable Quality Control, Maritsa Vegetable Crops Research Institute, 4003 Plovdiv, Agricultural Academy, Bulgaria*

Received: February 13, 2024; Revised: December 10, 2024

The experiment was carried out in the period 2018-2020 on the territory of the seed company "Superior D.R" in Velika Plana, Republic of Serbia, with six varieties of sweet pepper grown under greenhouse and open field conditions. The effect of genotype and method of cultivation on mechanical properties related to the textural characteristics was evaluated. The laboratory tests were conducted by the TA.XT Plus texture analyzer. The obtained force-deformation curves were analyzed for yield force, rupture force, modulus of flesh elasticity and deformation work. The cellulose content was also measured, but no significant correlations with the textural parameters of the fruits were found. The results of two-way analysis of variance indicated that the growing mode had an impact on modulus of flesh elasticity (29.73%), rupture force (11.09%) and yield force (10.68%). A significant influence of the genotype was recorded on the dynamic of rupture force (47.43%), modulus of flesh elasticity (25.60%) and deformation work (33.82%). Established genetic determination combined with an appropriate method of cultivation will be a good basis for successful breeding aimed at improving of the textural characteristics of pepper.

Keywords: *Capsicum annuum* L., yield force, rupture force, elasticity, deformation work, field, greenhouse

INTRODUCTION

Sweet pepper is a traditionally preferred vegetable in Serbia. The numerous specifics and the excellent adaptation to the local ecological conditions make the country very advantageous for growing pepper as this culture adapts perfectly to its climatic conditions and ecological factors [1].

Pepper fruits display high antioxidant activity determined by gallic acid equivalents. Many compounds are potential contributors to the total antioxidant capacity including ascorbate, flavonoids, carotenoids, phenolics and capsaicinoids [2]. Among the four maturity stages (immature green, green, immature red and red), the red one possesses enhanced functional properties [3]. Pepper is consumed both fresh and processed. Freshly chopped pepper must have an attractive appearance, an acceptable aroma, a suitable texture and a positive nutritional appearance to motivate initial and continuous purchases by consumers [4]. According to Beaulieu *et al.* [5] consumers often buy the first time based on appearance but repeated purchases are guided by expected quality factors determined by aromatic compounds and texture. Food texture can be evaluated by sensory analysis and by physical and mechanical properties of the foods. The second method is more consistent and is generally free from human factors [6].

Texture is the result of complex interactions between nutrients at the microstructure level and at higher structural levels such as tissue structure (cellular orientation, porosity) and the different types of tissues or organs that make up the nutrients [7]. Crispy textures are especially important in vegetables as consumers associate them with freshness and health [8]. Crispness is more suitable for wet vegetables consisting of living plant cells [9]. Both the cell wall strength of pepper fruits and the turgor pressure of pepper are related to characteristics such as hardness, fragility and crunching. These living cells have the property of turgor and intracellular pressure acting out against the cell wall which is balanced by another in force imparted by the hardness and elasticity of the cell wall [10]. According to Bourne [11] the textural properties of pepper are a group of physical characteristics affecting the structural elements of food and are felt when touched. They are also associated with the deformation and disruption of the structure of food under the action of force. They can give an objective assessment of the behavior of the pepper fruits after thermal, chemical or mechanical treatment [12].

During the warm months of the year pepper in the Republic of Serbia is grown both in polyethylene greenhouses and outdoor [13]. Decreased fruiting in pepper is common when daily temperatures are over

E-mail: *gpevicharova@abv.bg*

32°C [14]. Excessive temperatures lead to quality losses, e.g., alterations in form, color and texture of pepper fruits [15]. By reduced light intensity, the height of the plant, the number of nodes and the size of the leaves increase. In traditional areas pepper production in greenhouses is expanding to prevent yield reductions [16].

The aim of the present study was to evaluate the effect of genotype and method of cultivation on mechanical properties related to the textural characteristics of sweet pepper *Capsicum annuum* L.

EXPERIMENTAL

Method of cultivation

The experiment was conducted in the period 2018-2020 on the territory of the seed company "Superior D.O.O" in Velika Plana, the Republic of Serbia. Two variants of cultivation were applied: in plastic greenhouses and outdoor in five replicates. The seedlings were transplanted into greenhouses in the first ten days of May and into an open field in the second ten days of the same month. Standard agronomic practices such as fertilization and plant protection were used during the cultivation period. The plants were harvested at botanical maturity in early August from the greenhouse and in late August from the field.

Plant material

Six sweet pepper cultivars of *kapia* type were grown in the experiment. Four of them were Serbian (Slonovo uvo, Prizrenka, Belo uvo, Emina) and one (Ivailovska kapia) originated from Bulgaria. Italian variety Corno di Toro Rosso with horn-shaped fruits was also included in the study due to its widespread use in the production of ajvar in the Republic of Serbia.

Physical and chemical analyses

Textural parameters were studied one day after harvesting. The fruits for analyses were selected on the base of minimum variation in shape, color, size and firmness. They were cut longitudinally into strips of constant length. The laboratory tests were conducted by the TA.XT Plus texture analyser (Stable Micro Systems, UK) equipped with a heavy duty platform (HDP/90) with holed plate and a 2 mm diameter stainless steel puncture probe (SMS P/2) (Fig. 1). The instrument was set at a test speed of 2 $mm.s^{-1}$ and a travel distance of 10 mm. The analysis was performed on 5 individual fruits of each cultivar and method of cultivation. The measurement was done in the middle part of the longitudinal slices with skin. The force-deformation curves were analyzed for yield force (1st force maximum), modulus of flesh elasticity (slope up to 2nd maximum), deformation work (area under the curve up to 2nd maximum) and rupture force (force maximum) (Fig. 2).

Fig. 1. TA.XT texture analyzer

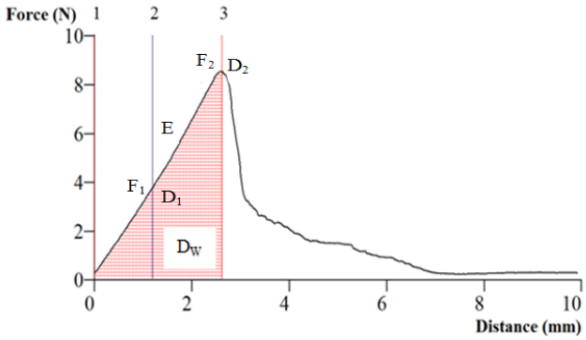

Fig. 2. Typical force-distance curve of the fresh pepper tissue. F_1 - Yield force [N]]; D_1 -Yield deformation [mm]; F_2 - Rupture force (firmness) [N]; D_2 - Rupture deformation [mm]; Y - Modulus of flesh elasticity $[N.mm^{-1}] = F_2 / (D_2\text{-}D)$; Dw - Deformation work [N.mm] $= \int_{D_0}^{D_2} F \cdot D_D$.

The cellulose content was measured on the same five fresh whole pepper fruits from each variant using Henneberg-Stohman method [17].

Data analyses

Significant differences in the studied characters of pepper genotypes were determined by Duncan's multiple range test ($P<0.05$). A two-way analysis of variance was applied to evaluate the effect of genotype, method of cultivation and their interaction on the analyzed traits. Pearson correlation coefficients were estimated in order to examine the relationships between the studied parameters. Coefficient of variability (CV) and standard deviation (sd) were also calculated. All data analyses were performed using the SPSS-16 software.

RESULTS AND DISCUSSION

The obtained force-distance curves of fresh pepper tissue had a specific design for each of the genotypes (Fig. 3).

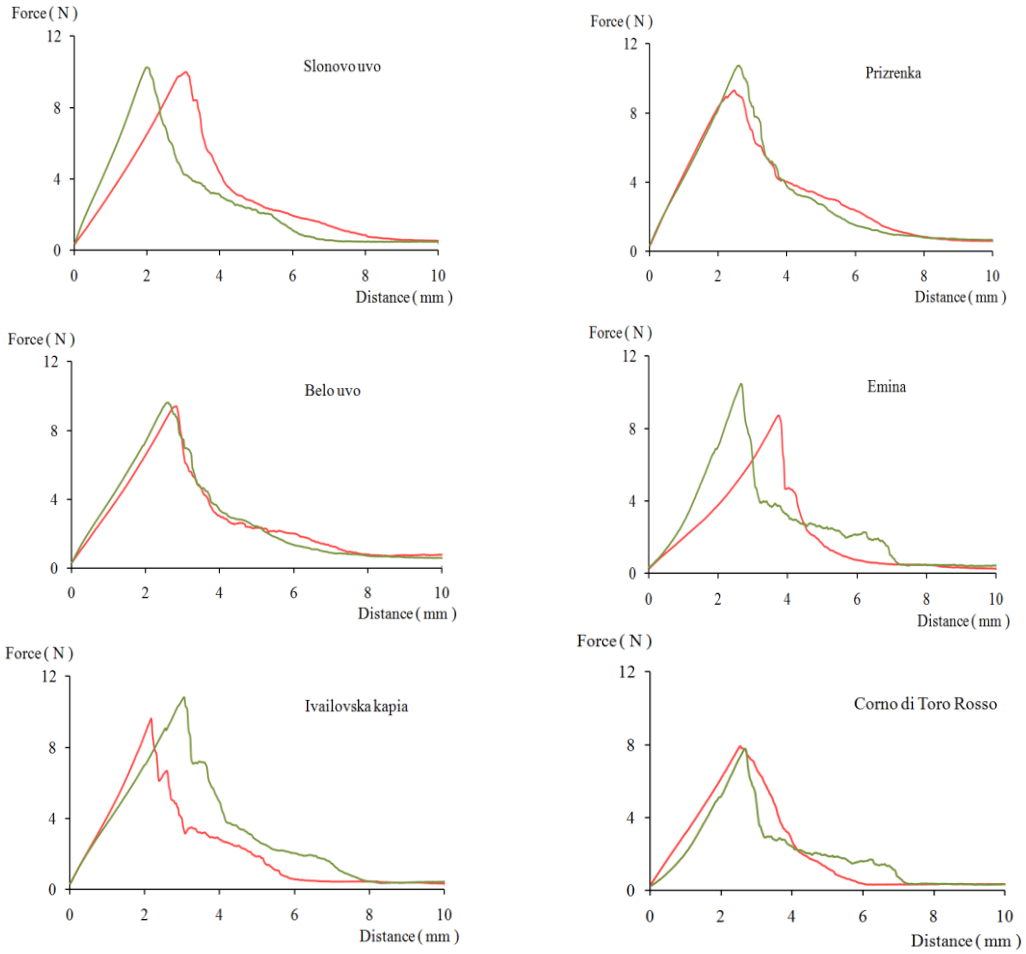

Fig. 3. Force-distance curves of fresh pepper tissue obtained from field (–) and greenhouse fruits (–)

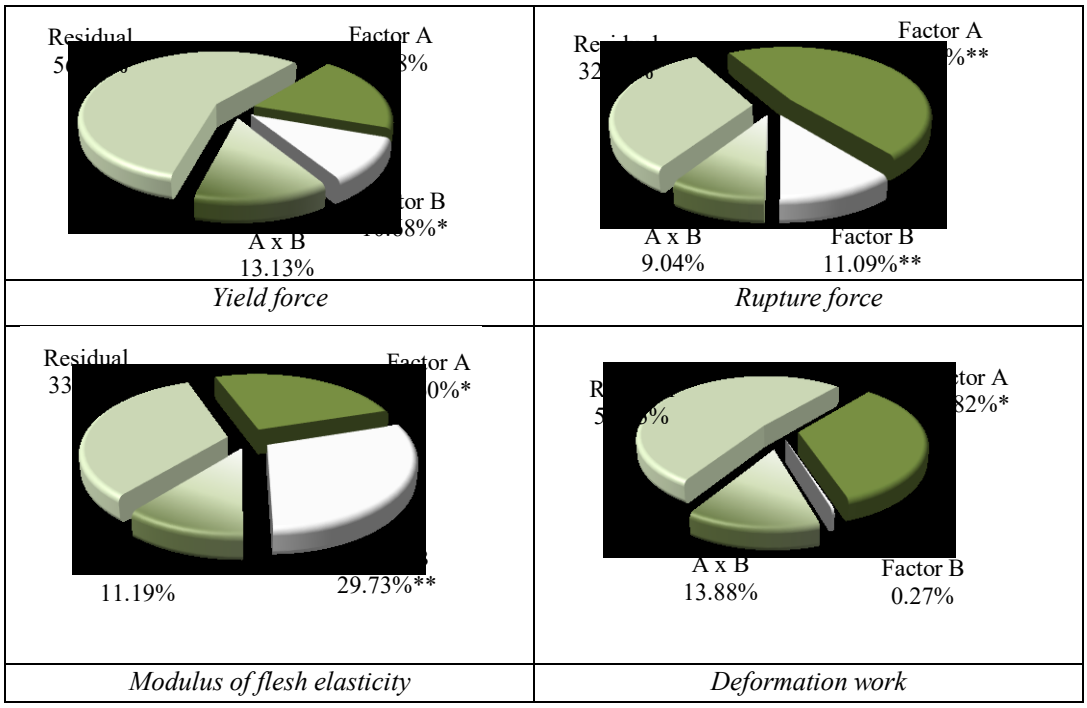

Fig. 4. Effect of genotype (factor A) and method of cultivation (factor B) on the studied mechanical parameters in pepper

Most of the investigated pepper varieties grown under field conditions were characterized by a lower curve maximum compared to those grown in the greenhouse. Belo uvo and Corno di Toro Rosso had

close positions of the maximum peak and very similar type of the curves describing both cultivation methods. The initial slope of the force-distance curves for Slonovo uvo and Emina as field production were much less steep than the curves defining greenhouse production.

Genotypic differences with respect to yield force were better expressed in pepper fruits from the field (Table 1). Variety Emina had the lowest value compared to the other varieties. The fruits of the pepper varieties grown in the greenhouse did not differ significantly in the studied mechanical parameter. Low CV levels for both variants were observed.

Higher values of rupture force with the exception of Corno di Toro Rosso were recorded in the varieties grown under greenhouse conditions indicating higher resistance to mechanical damage of pepper tissue. The studied textural parameter was also genetically determined. Statistical differences were proved between the variety of horn-shaped fruits and the group of five *kapia* type varieties in the greenhouse and four ones in the field. As a whole, the investigated varieties of *kapia* type formed harder fruits in greenhouse plants.

Modulus of flesh elasticity shows how easily a specimen can be deformed. All genotypes grown under greenhouse conditions were characterized by higher modulus of flesh elasticity values than those grown under field conditions. This means that their fruits were stiffer and more resistible to plastic deformation. A genetic expression was observed in both cultivation methods. The lowest values of the modulus of flesh elasticity were recorded in Emina from the field and in Corno di Toro Rosso from the greenhouse. Relatively low CV values (below 11%) characterized the variation between varieties as slight. Deformation work was the most variable inter-variety parameter with CV over 11 percent regardless of the cultivation method. Italian variety Corno di Toro Rosso seemed to absorb less energy for the deformation before fracture of the fruit tissue than the *kapia* type varieties. The most difficult to deform were the pepper fruits of Slonovo uvo, Prizrenka and Emina from the field and fruits of Prizrenka and Ivailovska kapia from the greenhouse.

The information obtained about the pepper texture profile revealed lower values of the coefficient of variability in the investigated mechanical parameters for the field variant. It was better expressed in terms of deformation work.

Higher influence by the genotype than by the method of cultivation was recorded on the dynamics of the deformation work and the rupture force (Fig. 4).

A significant very close impact of the genotype (25.60%) and the method of cultivation (29.73%) on the modulus of flesh elasticity was established. The growing mode did not impact on the deformation work. The influence of the interaction between both factors on the studied mechanical parameters was insignificant.

Generally, the results of two-way analysis of variance indicated that the method of cultivation could change the elasticity and the firmness of the pepper fruits. The comparatively high values of the residual factor could be explained by the influence of other factors on the texture parameters such as turgor cell pressure, pectin in cell wall, lamella, etc., that were not a subject of this study.

The mechanical parameters of fruits and vegetables depend on the cell arrangement in the tissue, especially on cell dimension and cell wall structure. Some part of this variation can be expressed by crude fiber content [18]. Tissue firmness has its source in the cell walls and their carbohydrate cellulose, hemi-cellulose including pectic substances [19]. It is presented as the major fiber constituent in most of the foods [20]. Cellulose gives plants the necessary strength and elasticity. This was the main reason to analyze the content of cellulose in the pepper fruits and to search for a relationship with the textural parameters in the studied pepper varieties.

Genotypic reaction regarding the cellulose content in pepper fruits was observed in both methods of cultivation (Fig. 5).

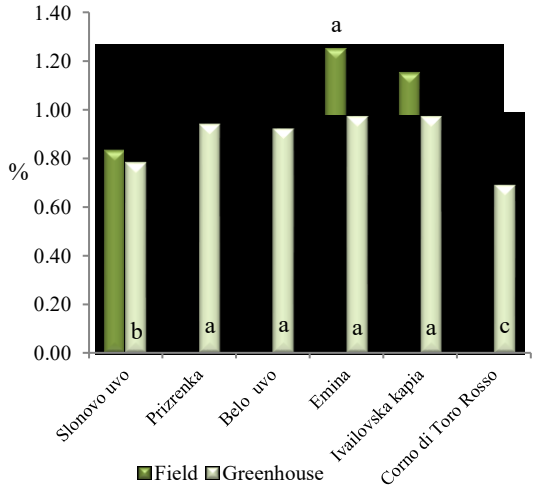

a,b… Duncan's multiple range test (P<0.05)

Fig. 5. Cellulose content of pepper fruits grown under field and greenhouse conditions

It was better expressed in pepper fruits from the greenhouse. Varieties Emina and Ivailovska kapia had the highest values of cellulose regardless of the

growing procedure. However, these varieties did not display the highest values of the studied mechanical parameters (Table 1). The correlation coefficients showing the relationship between the cellulose content and the textural parameters in the field fruits were not significant (Table 2). A moderate correlation was proved for the modulus of flesh elasticity and rupture force in the greenhouse variant. The lack of significant correlations between the cellulose content and the measured texture parameters could be explained by the structure of the pepper fruits. According to Mohsenin [6] the test specimen should ideally be isotropic and homogeneous**.** In reality, all plant food materials are cellular composite structures formed by the accumulation of fibers and are therefore inherently inhomogeneous and anisotropic [21]. Another probable reason in the experiment may be due to the difference in the parts of the pepper fruits that were involved in the measurement. The mechanical parameters were determined in the middle area of the longitudinal slices. In contrast, the cellulose content was analyzed after a fairly good homogenization of the whole pepper fruit material.

Table 1. Textural parameters of the studied pepper cultivars

Cultivar	Yield force (N)	Rupture force (N)	Modulus of flesh elasticity ($N.mm^{-1}$)	Deformation work (N.mm)
Field				
Slonovo uvo	4.275^{a}	9.995^{a}	4.682^{ab}	13.527^{a}
Prizrenka	4.085^{a}	9.328^{a}	4.403^{ab}	12.717^{a}
Belo uvo	4.281^{a}	9.419^{a}	4.752^{ab}	11.532^{ab}
Emina	3.501^{b}	8.718^{ab}	3.813^{b}	12.667^{a}
Ivailovska kapia	4.126^{a}	9.631^{a}	4.919^{a}	11.542^{ab}
Corno di Toro Rosso	3.998^{a}	7.918^{b}	4.040^{ab}	9.536^{b}
Mean ($\bar{x}$ ± sd)	4.044 ± 0.288	9.168 ± 0.742	4.435 ± 0.433	11.920 ± 1.397
CV (%)	7.12	8.09	9.77	11.72
Greenhouse				
Slonovo uvo	4.123^{ns}	10.260^{a}	5.550^{a}	11.087^{ab}
Prizrenka	4.243^{ns}	10.762^{a}	5.401^{a}	13.268^{a}
Belo uvo	4.694^{ns}	9.624^{a}	5.310^{a}	10.414^{ab}
Emina	4.300^{ns}	10.468^{a}	5.429^{a}	11.954^{ab}
Ivailovska kapia	4.850^{ns}	10.825^{a}	5.266^{a}	13.817^{a}
Corno di Toro Rosso	3.939^{ns}	7.775^{b}	4.049^{b}	8.848^{b}
Mean ($\bar{x}$ ± sd)	4.358 ± 0.347	9.952 ± 1.151	5.168 ± 0.557	11.565 ± 1.847
CV (%)	7.96	11.57	10.77	15.97

^{a,b}… Duncan's multiple range test ($P<0.05$); ^{ns} - not significant

Table 2. Correlation analysis of the studied pepper properties

	C (F)	C(G)	YF (F)	YF (G)	DW (F)	DW (G)	MFE(F)	MFE (G)	RF (F)	RF (G)
C (F)	♦									
C(G)	0.276	♦								
YF (F)	-0.447	-0.152	♦							
YF (G)	0.087	0.249	0.403	♦						
DW (F)	0.157	-0.307	0.185	0.245	♦					
DW (G)	0.097	-0.036	0.214	0.544^{*}	0.819^{**}	♦				
YM (F)	-0.199	0.460	-0.218	-0.224	-0.865^{**}	-0.715^{**}	♦			
YM (G)	-0.051	0.551^{*}	-0.384	-0.317	-0.779^{**}	-0.700^{**}	0.948^{**}	♦		
RF (F)	-0.212	0.432	0.129	-0.016	-0.097	-0.075	0.543^{*}	0.553^{*}	♦	
RF (G)	0.065	0.540^{*}	-0.157	0.401	0.296	0.559^{*}	0.045	0.148	0.525^{*}	♦

C - cellulose; YF - yield force; DW – deformation work; MFE–modulus of flesh elasticity; RF – rupture force; F - field; G - greenhouse

Simple correlations between the studied textural parameters were evaluated (Table 2).

A very strong positive correlation (r = 0.948) was found between the moduli of flesh elasticity recorded in field and greenhouse fruits. A strong positive correlation (r = 0.819) was established between deformation work measured in the field fruits and in the greenhouse ones. The high values of these coefficients of correlation show that the above-mentioned textural parameters were changed regularly in both studied methods of cultivation.

Negative strong correlations were recorded between modulus of flesh elasticity and the deformation work regardless of the cultivation method. The other correlations ranged from weak to moderate and did not actually have any practical application. Hence, none of the studied mechanical parameters can be used as a primary indicator for determining the quality of the texture of the pepper fruits.

CONCLUSION

In the present experiment, it was established that the method of cultivation could change some of the investigated mechanical parameters. Positive effects of greenhouse crop growing were observed in modulus of flesh elasticity and rupture force. Pepper fruits of *kapia* type were harder, stiffer and more resistible to plastic deformation than the ones grown under field conditions. The studied parameters were also genetically determined, which is a good basis for successful breeding aimed at the improving the textural characteristics of pepper.

REFERENCES

1. Z. Ilić, Z. Krivošej, L. Amiđžić, D. Milinčić, *Acta Hortic.,***462**, 143 (1997).
2. C. Fraga, P. Oteiza, M. Galleano, *Biochim. Biophys. Acta,* **1840**, 931 (2014).
3. N. Deepa, Ch. Kaur, B. George, B. Singh, H. Kapoor, *LWT*, **40**, 121 (2007).
4. R. Shewfelt, *Postharvest Biol. Technol.*, **15**, 197 (1999).
5. J. C. Beaulieu, D. A. Ingram, J. M. Lea, K. L. Bett-Garber, *J. Food Sci.,***69**, 250 (2004).
6. N. Mohsenin, Physical Properties of Pim and Animal Materials, Gordon and Breach Science Publishers, New York, 1986.
7. J. M. Aguilera, D. W. Stanley, Microstructural Principles of Food Processing and Engineering, Aspen Publishers, Gaithersburg, 1999.
8. L. Fillion, D. Kilcast, *Food Qual. Prefer.,* **13**, 23 (2002).
9. J. F. V. Vincent, *J. Sci. Food Agric.,***78**, 162 (1998).
10. M. D. Alvarez, D. E. Saunders, J. F. V. Vincent, G. Jeronimidis, *J. Texture Stud.*, **31**, 457 (2000).
11. M. C. Bourne, *J. Food Sci.,***47**, 440 (1982).
12. I. Bakalov, Z. Manev, T. Petrova, M. Ruskova, K. Ivanova, G. Zsivanovits, *J. Mt. Agric. Balk.,* **21**, 277 (2018).
13. Z. Ilić, L. Milenković, L. Šunić, D. Cvetković, E. Fallik, *J. Sci. Food Agric*., **95**, 2660 (2015).
14. I. Rylski, M. Spigelman, *Sci. Hortic*., **29**, 31 (1986).
15. T. Geissler, Gemüseproduktion unter Glas und Plasten, VEB Deutscher Landwirtschaftsverlag, Berlin, 1985.
16. Z. Ilić, L. Milenković, M. Đurovka, N. Kapoulas, 46th Croatian and 6th Int. Symp. on Agric., Opatija, 2011.
17. A. Genadiev, D. Kalcheva, N. Nenchev, N. Tevekeliev, N. Chavdarova, Food Analyses, Technique, Sofia, 1969.
18. J. Blahovec, *J. Mater. Sci.*, **23**, 3588 (1988).
19. J. P. Van Buren, *J. Texture Stud.,***10**, 1 (1979).
20. B. Rani, A. Kawatra, *Plant Foods Hum. Nutr.*, **45**, 343 (1994).
21. A. G. Atkins, Y. W. Mai, Elastic and plastic fracture: metals, polymers, ceramics, composites, biological materials, Halsted Press, New York, 1985.

Bulgarian Chemical Communications, Volume 57, Issue 1 (pp. 26-31) 2025 *DOI: 10.34049/bcc.57.1.5654*

Solid-liquid phase equilibrium in the LiBr-$CaBr_2$-H_2O system at 35 ºC and 50ºC

C. Christov[1*], T. Tsenov[1], N. Ivanova[2], S. Donchev[1]

[1]*Department of Chemistry, Faculty of Natural Sciences, Shumen University "Konstantin Preslavski", 115, Universitetska Str., 9700 Shumen, Bulgaria*
[2]*Department of Chemistry, Medical University Pleven, Pleven, Bulgaria*

Received: July 10, 2024; Revised: January 21, 2025

The investigation of the phase diagrams of lithium bromide mixed systems is of practical importance with a view to explain the distribution of bromide ions in natural evaporated deposits during crystallization of salts as a result of sea water evaporation, during treatment of natural deposits, production of bromide mineral resources, and especially in improvement of the technology for extraction of lithium from brine deposits. In this study, the solubility of bromide minerals in the mixed system LiBr-$CaBr_2$-H_2O was investigated at 35 ºC and 50 ºC by physico-chemical analysis. The compositions of the thoroughly suction-dried solid phases were specified by the Schreinemakers graphic method. At T=35ºC the equilibrium crystallization of LiBr.$2H_2O$ (cr), LiBr.H_2O (cr), $CaBr_2$.$4H_2O$ (cr) and $CaBr_2$.$2H_2O$ (cr). was established. At T = 50ºC precipitation of LiBr.H_2O (cr), $CaBr_2$.$4H_2O$ (cr) and $CaBr_2$.$2H_2O$ (cr). was established. The solubility of lithium bromide solids sharply decreases in a ternary system with added calcium bromide solids at both temperatures. It was concluded that the phase transition temperature (PPT) LiBr.$CaBr_2$.$5H_2O$ (cr) → LiBr.H_2O (cr) + $CaBr_2$.$4H_2O$ (cr) lies in the temperature range from 25ºC to 35ºC.

Keywords: phase equilibrium; bromide minerals solubility; mixed system LiBr-$CaBr_2$-H_2O

INTRODUCTION

The behavior of bromide as a trace element in vaporizing seawater and the diagenetic reactions of evaporates are of prime importance for geochemical studies on marine chemical sediments [1-4]. The experimental and thermodynamic modeling investigation of the phase diagrams of lithium bromide mixed systems is of practical importance with a view to explain the distribution of bromide ions in natural evaporated deposits during crystallization of salts as a result of sea water evaporation, during treatment of natural deposits, production of bromide mineral resources, and especially in improvement of the technology for extraction of lithium from brine deposits [5-9].

In recent years, there has been a noticeable increase in lithium production due to the growing interest in this valuable resource, which aligns with the escalating demand for electric vehicles and cordless consumer electronics. Lithium is used for the production of lithium-ion batteries, in ceramics and glass, lubricants, polymer production, and air conditioning. The production of lithium batteries is expected to increase in the coming years due to the decarbonization of key markets [9-11]. With the rapidly developing new energy industry in the world the global demand for lithium resources continually grows. The demand for lithium carbonate is expected to increase from 265 kt in 2015 to 498 kt in 2025. The most efficient and cost-effective way to produce lithium is from brines. The extraction from brine, however, carries great environmental risks due to the large consumption of water and the pollution of underground sources of drinking water [12, 13]. Experimental and theoretical studies on solid-liquid phase equilibrium in mixed lithium systems in combination with major ocean cations (Na^+, K^+, Mg^+, Ca^+), halide (Cl^-, Br^-, I^-), and sulfate (SO_4^{2-}) mixed systems at temperatures ranging from 0ºC to 50ºC are of high importance in improvement of the technology for extraction of lithium from brine deposits [5-8, 9-11].

The need to determine the required conditions for extracting lithium from natural brines and salt deposits of the marine type constitutes the motivation behind the study of aqueous solutions of lithium and magnesium, and calcium halides over a wide temperature range. The solubility data for lithium–magnesium chloride/bromide (1-1 + 2-1) mixtures of the type LiX-MgX_2-H_2O (X=Cl, Br) are available in a temperature range from 0º to 75ºC. According to these data a lithium carnallite double salt (LiCl.$MgCl_2$.$7H_2O$ (cr)) precipitates from saturated chloride solutions [3, 5, 14].

* To whom all correspondence should be sent:
E-mail: *ch.christov@shu.bg; christovshumen@gmail.com*

According to the data, the lithium and magnesium bromide ternary system is of simple eutonic type at temperatures ranging from 25°C to 75°C [5, 7, 14]. The experimental solubility data for LiCl-$MgCl_2$-H_2O, and LiBr-$MgBr_2$-H_2O systems are also validated by development of the Pitzer approach thermodynamic solid liquid equilibrium model at standard temperature [5], and at T = 75°C [7] for the lithium-magnesium bromide system. The experimental data for LiX-CaX_2-H_2O (X=Cl, Br) systems are scarce. Solubility data for the chloride system are available from 0°C to 50°C. According to these data a double salt with stoichiometry 1-1-5 (LiCl.$CaCl_2$.5H_2O (cr)) precipitates in the ternary system at 0°, 10°, and 25°C [6, 11]. There is no field of equilibrium crystallization of the double salt LiCl.$CaCl_2$.5H_2O (cr) at 40° and 50°C (see Fig. 6 in ref. [11]). The solubility data for the LiBr-$CaBr_2$-H_2O system are available only at standard temperature. In a previous study [6] we corrected the available solubility data [14] for this bromide system. Precipitation of the double salt LiBr.$CaBr_2$.5H_2O (cr) has been established at 25°C. The experimental solubility data at standard temperature for the LiBr-$CaBr_2$-H_2O system are also validated by development of a thermodynamic solid liquid equilibrium model [6]. Precipitation of the double salt LiBr.$CaBr_2$.5H_2O(cr) was also fully confirmed by the solubility study of Cui *et al.* [9] at 25°C. In this study we determined the solubilities in the LiBr-$CaBr_2$-H_2O system at 35°C and 50°C. The reported new solubility data are of high importance for development of an accurate T-variable (from 0°C to 50°C) solid-liquid equilibrium thermodynamic model for lithium bromide rich brines, and therefore in improvement of the technology for extraction of lithium resources from brine deposits.

EXPERIMENTAL

In this study, the bromide minerals' solubility in the mixed system LiBr-$CaBr_2$-H_2O was investigated at T = (35 and 50) °C. The solubility of bromide minerals in the ternary system was studied by the method of isothermal decrease of the supersaturation [1, 4-7, 15, 16]. Different weight ratios of solid LiBr, and $CaBr_2$ were used for each experiment. Crystal salts in excess of the solubilities at T=(35 and 50) °C were mixed with water. The solution was heated until the solid phases were completely dissolved and then transferred to a double-walled glass thermostat and cooled rapidly to the desired temperature of 35°C and 50°C. The quick cooling of the solution, followed by agitation with a magnetic stirrer, ensured a fast decrease of the supersaturation. Equilibrium was attained by continuous stirring for 24 h.

The solid lithium bromide and calcium bromide samples were from Fluka with mass fraction purity of 0.999. The solids were used without further purification. Samples of the liquid and wet solid phases were withdrawn for analysis. Their separation has been achieved by a Cooch filter (G-3). Weighed amounts of the liquid and the wet solid phase were diluted to a definite volume and analyzed for determining solution composition. The compositions of the saturated solutions and the corresponding wet solid phase were established using the methods described in our previous studies [1-3, 6, 16]. Calcium ion was determined by complexometric titration with Eriochrome black T as indicator [6, 17]. Merck ammonium buffer solution (ammonium chloride/ammonia) was used for maintaining the high pH (pH = 10-11) of solutions in the complexometric titration process [6]. The amount of bromide was found by titration with silver nitrate solution (the Mohr method) [17, 6]. The concentration of lithium ion [Li^+] was calculated by the balance reaction: $[Li^+] = [Br^-]_{total} - 2x[Ca^{2+}]$ [6, 16]. The compositions of the thoroughly suction-dried solid phases were specified by the Schreinemakers' graphic method [18], see also refs. [1, 2, 6, 16].

RESULTS AND DISCUSSION

The results from the solubility measurements in the LiBr-$CaBr_2$-H_2O system are presented in Table 1 and Figure 1, and Table 2 and Figure 2 at T = 35 °C, and T=50 °C, respectively. The experimental error is within the range of ± (0.1 to 0.3) per cent. Each experimental result represents the arithmetical mean of three parallel determinations.

Table 1. Experimental mass fraction *w* and molality solubility of lithium and calcium bromide solid phases in the (m_1LiBr + m_2CaBr_2) (aq) system at T = 35°C

Liquid phase, 10^2 *w*		Liquid phase, molality (m/mol·kg^{-1})		Wet solid phase, 10^2 *w*		Solid phase
LiBr	$CaBr_2$	LiBr	$CaBr_2$	LiBr	$CaBr_2$	
62.5	0.0	19.2	0.0	66.3	0.0	LiBr.2H_2O (cr)
57.9	5.80	18.3	0.80	69.8	1.31	LiBr.2H_2O (cr)
50.7	13.8	16.5	1.94	65.7	3.20	LiBr.2H_2O (cr)
47.3	18.3	15.8	2.66	66.9	3.19	LiBr.2H_2O (cr)
42.3	23.4	14.2	3.41	65.6	4.30	LiBr.2H_2O (cr)
40.7	27.1	14.6	4.21	76.7	5.03	LiBr.H_2O (cr)
37.2	30.0	13.1	4.58	72.1	7.10	LiBr.H_2O (cr)
32.9	34.5	11.6	5.29	59.1	16.0	LiBr.H_2O (cr)
31.9	38.2	12.3	6.39	72.7	7.58	LiBr.H_2O (cr)
28.8	41.7	11.2	7.07	64.9	10.3	LiBr.H_2O (cr)
27.9	43.3	11.2	7.52	72.4	10.4	LiBr.H_2O (cr)
26.6	44.7	10.7	7.79	60.4	16.9	LiBr.H_2O (cr)
25.0	46.4	10.1	8.12	42.5	36.1	E[a]
24.5	46.9	9.86	8.20	41.1	38.6	E[a]
24.8	47.2	10.2	8.43	17.8	62.9	E[a]
24.1	47.7	9.84	8.46	36.8	42.9	E[a]
23.2	48.5	9.4	8.56	3.53	76.9	$CaBr_2$.2H_2O(cr)
21.5	50.7	8.91	9.12	7.80	71.2	$CaBr_2$.2H_2O(cr)
18.1	52.8	7.16	9.08	8.1	69.0	$CaBr_2$.2H_2O(cr)
14.9	54.2	5.55	8.78	10.5	59.6	$CaBr_2$.4H_2O(cr)
12.1	56.8	4.48	9.14	3.85	67.4	$CaBr_2$.4H_2O(cr)
9.70	58.4	3.50	9.16	2.85	68.1	$CaBr_2$.4H_2O(cr)
6.97	60.6	2.47	9.35	0.93	71.5	$CaBr_2$.4H_2O(cr)
4.90	62.0	1.70	9.37	0.81	70.9	$CaBr_2$.4H_2O(cr)
2.80	63.8	0.97	9.56	0,98	70.2	$CaBr_2$.4H_2O(cr)
0.0	66.1	0.0	9.76	0.0	71.2	$CaBr_2$.4H_2O(cr)

[a]E = LiBr.H_2O (cr)+ $CaBr_2$.2H_2O (cr)

Table 2. Experimental mass fraction *w* and molality solubility of lithium and calcium bromide solid phases in the (m_1LiBr + m_2CaBr_2)(aq) system at T = 50°C

Liquid phase, 10^2 *w*		Liquid phase, molality (m/mol·kg^{-1})		Wet solid phase, 10^2 *w*		Solid phase
LiBr	$CaBr_2$	LiBr	$CaBr_2$	LiBr	$CaBr_2$	
65.9	0.0	22.2	0.0	74.6	0.0	LiBr.H_2O (cr)
60.5	5.59	20.5	0.83	73.1	2.90	LiBr.H_2O (cr)
57.3	9.60	19.9	1.45	74.0	3.80	LiBr.H_2O (cr)
53.4	13.5	18.6	2.04	69.6	7.10	LiBr.H_2O (cr)
43.7	25.8	16.5	4.23	67.1	10.3	LiBr.H_2O (cr)
38.6	31.5	14.8	5.25	55.9	19.8	LiBr.H_2O (cr)
33.9	37.2	13.5	6.44	53.5	22.2	LiBr.H_2O (cr)
28.9	42.8	11.7	7.56	41.8	32.4	LiBr.H_2O (cr)
27.5	45.1	11.6	8.26	38.1	53.4	E[a]
27.0	46.1	11.6	8.57	26.9	59.8	E[a]
26.8	46.0	11.4	8.46	19.2	68.4	E[a]
25.5	47.9	11.0	8.99	7.50	74.3	$CaBr_2$.2H_2O(cr)
22.2	50.5	9.36	9.25	5.20	75.8	$CaBr_2$.2H_2O(cr)
16.9	55.4	7.0	9.98	3.10	78.1	$CaBr_2$.2H_2O(cr)
12.4	59.5	5,07	10.6	2.40	80.9	$CaBr_2$.2H_2O(cr)
6.00	64.9	2.37	11.2	3.10	71.8	$CaBr_2$.4H_2O(cr)
2.68	67.2	1.02	11.1	0.90	73.1	$CaBr_2$.4H_2O(cr)
0.0	70.2	0.0	11.8	0.0	72.6	$CaBr_2$.4H_2O(cr)

[a]E = LiBr.H_2O (cr)+ $CaBr_2$.2H_2O (cr)

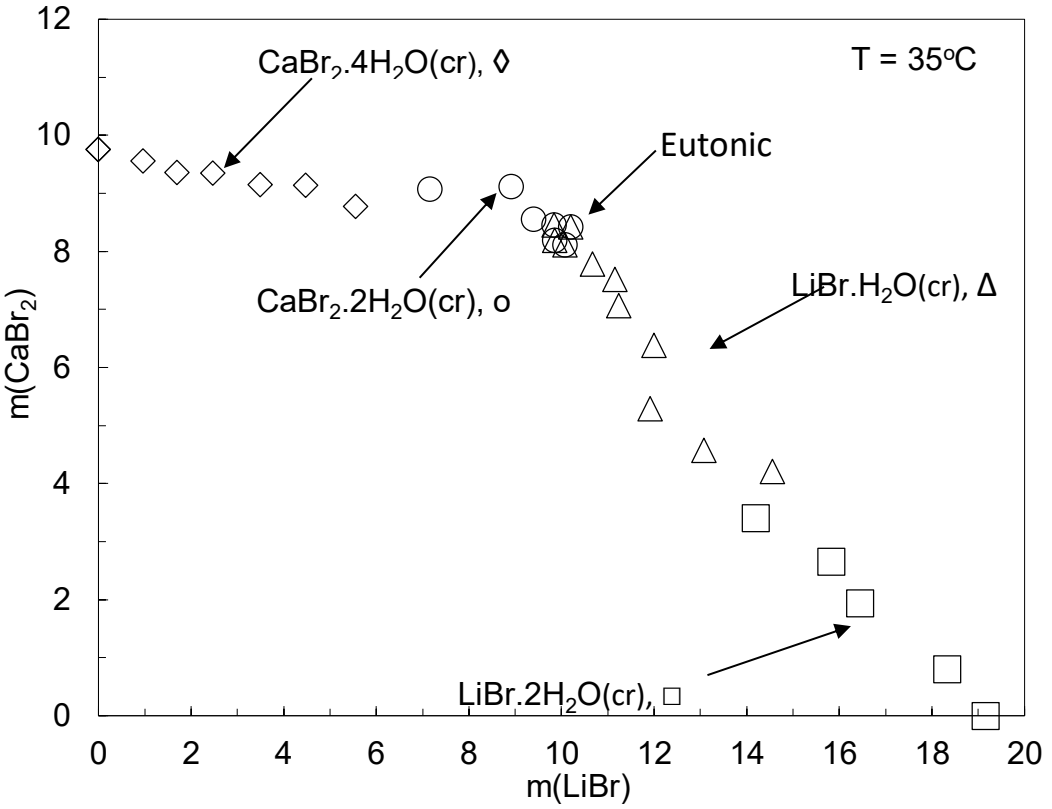

Fig. 1. Experimental molality solubility (mol.kg^{-1}) of $LiBr.2H_2O$ (cr) (open squares), $LiBr.H_2O$ (cr) (open triangles), $CaBr_2.4H_2O$ (cr) (open diamonds), and $CaBr_2.2H_2O$ (cr) (open circles) in the system LiBr-$CaBr_2$-H_2O at T=35°C

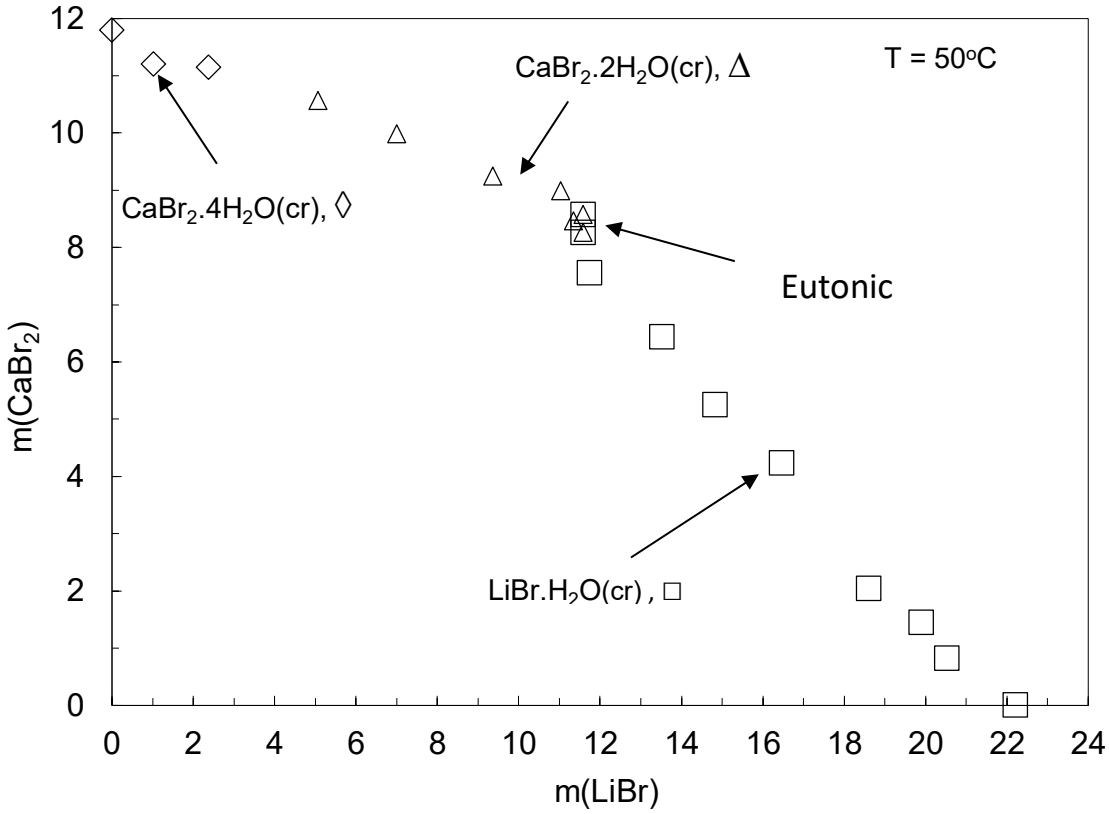

Fig. 2. Experimental molality solubility (mol.kg^{-1}) of $LiBr.H_2O$ (cr) (open squares), $CaBr_2.4H_2O$ (cr) (open diamonds) and $CaBr_2.2H_2O$ (cr) (open triangles) in the system LiBr-$CaBr_2$-H_2O at T=50°C

The data presented on Tables 1 and 2, and Figs. 1 and 2 show that the solubilities of lithium bromide and calcium bromide solids in binary systems sharply increase with temperature. According to data $LiBr.2H_2O$ (cr) and $LiBr.H_2O$ (cr) precipitate in binary system LiBr-H_2O at 35 °C, and 50°C, respectively. The determined here solubility of $LiBr.H_2O$ (cr) in binary system at 50°C is very close to those reported in a previous experimental study [5]. According to data presented on Tables 1 and 2, and Figs. 1 and 2 $CaBr_2 \cdot 4H_2O$ (cr) crystallized in the binary system $CaBr_2$-H_2O at both temperatures. Precipitation of tetrahydrate is in agreement with the temperature variable model and recommendations given in the literature. According to the 0-100 °C solid-liquid equilibrium model of Christov [4] the ($CaBr_2 \cdot 6H_2O$ (cr) ↔ $CaBr_2 \cdot 4H_2O$ (cr)) phase transition in water is predicted to occur at a temperature of 32.1°C, which is only by 2.1 C lower than the transition temperature accepted in the compilation of Kirgintsev *et al.* [19] (34.2°C). The determined here solubility of $CaBr_2 \cdot 4H_2O$ (cr) in pure water at 50°C is very close to those reported in previous experimental studies [4, 16]. The determined here composition of precipitating calcium bromide solids ($CaBr_2.4H_2O$ at T=50°C), and concentration of saturated binary $CaBr_2$-H_2O solutions at both temperatures (T=35°C and T=50°C) are in excellent agreement with solubility measurements and thermodynamic phase equilibrium models at standard temperature [6], and in a wide range of temperatures from 0° to 100°C (see Fig. 2 in Christov [4]).

In the mixed system LiBr-$CaBr_2$-H_2O the equilibrium crystallization of $LiBr.2H_2O$ (cr), $LiBr.H_2O$ (cr), $CaBr_2.4H_2O$ (cr) and $CaBr_2.2H_2O$ (cr) has been established at 35°C. At T = 50°C precipitation of $LiBr.H_2O$ (cr), $CaBr_2.4H_2O$ (cr) and $CaBr_2.2H_2O$ (cr) has been determined. The solubilities of lithium bromide solids sharply decrease in ternary system with adding calcium bromide solids at both temperatures. According to data presented in Christov *et al*. [6] and in this study, the phase transition temperature (PPT) $LiBr.CaBr_2.5H_2O$ (cr) → $LiBr.H_2O$ (cr) + $CaBr_2.4H_2O$ (cr) lies within the temperature range from 25°C to 35°C. From the experimental data obtained in this study and modeling study presented in Lassin and André [11] it can be concluded that in both lithium-calcium halide systems LiCl-$CaCl_2$-H_2O and LiBr-$CaBr_2$-H_2O double salts with stoichiometry 1-1-5 precipitate only at low temperature below or equal to standard. According to the reference data [11] at T ≥ 40°C only simple salts precipitate from a saturated mixed lithium-calcium chloride system. According to the data presented in this study at T ≥ 35°C only simple salts precipitate from saturated mixed lithium-calcium bromide system.

There are several invariant point data given in Tables 1 and 2. Development of solid-liquid equilibria model for the mixed system LiBr-$CaBr_2$-H_2O is the best approach to determine which of these data points is the actual invariant point and to plot the solubility isotherms at 35°C and 50°C. Development of a solid-liquid equilibria model for mixed systems at constant temperature requires as a first step construction a not-concentration restricted models for corresponding binary subsystems. For the mixed system under study LiBr-$CaBr_2$-H_2O the experimental activity data for both binary subsystems (LiBr-H_2O and $CaBr_2$-H_2O) are available only at 25°C. These data are used to construct models for binaries and using our own solubility data to develop model for mixed system LiBr-$CaBr_2$-H_2O at 25°C (ref. 10). In this study we reported solubility data for LiBr-$CaBr_2$-H_2O at 35°C and 50°C. The reported data can be used to evaluate mixing Pitzer parameters and to develop a model for a mixed system only in case of availability of activity data for binary subsystems at 35°C and 50°C. The widely used temperature variable model for $CaBr_2$-H_2O described in a previous study of Christov [4] can be used in a model development for the mixed system LiBr-$CaBr_2$-H_2O. New low- and high-molality activity data for binary LiBr-H_2O at 35°C and 50°C are needed to develop a solid-liquid equilibrium model for the mixed system under study. The data presented here are a very good base to develop an accurate T-variable solid-liquid equilibrium thermodynamic model for lithium bromide-rich brines in the temperature range with importance for improvement of technology for extraction of lithium resources (from 0°C to 50°C).

Acknowledgement: *This study was supported by the European Regional Development Fund within the Operational Programme "Science and Education for Smart Growth 2014-2020" under the Project CoE "Universities for Science, Informatics and Technologies in e-Society (UNITe) BG05M2OP001-1.001-0004". The work of St. Donchev is also supported by the Bulgarian Ministry of Education and Science under the National Program "Young Scientists and Postdoctoral Students – 2".*

REFERENCES

1. C. Balarew, C. Christov, *Compt. rend. Acad. Bulg. Sci.,* **45**, 49 (1992). ISSN 2367-5535

2. C. Balarew, C. Christov, S. Petrenko, V. Valyashko, *J. Solution Chem.,* **22**, 173 (1993). https://doi.org/10.1007/BF00650683
3. C. Christov, C. Balarew, *J. Solution Chem.*, **24**, 1171 (1995). https://doi.org/10.1007/BF00972963
4. C. Christov, *Calphad,* **35**, 42 (2011). doi:10.1016/j.calphad.2010.11.001
5. C. Christov, C. Balarew, V. Valyashko, S. Petrenko, *J. Solution Chem.,* **23,** 595 (1994). DOI:10.1007/BF00972747
6. C. Christov, S. Velikova, K. Ivanova, *J. Chem. Thermodyn.,* **32**, 1505 (2000). doi:10.1006/jcht.2000.0688
7. C. Christov, *J. Chem. Thermodyn.,* **27**, 1267 (1995). https://doi.org/10.1006/jcht.1995.0133
8. C. Christov, *J. Chem. Thermodyn.,* **37**, 1036 (2005). https://doi.org/10.1016/j.jct.2005.01.008
9. R. Cui, C. Peng, G. Nie, S. Sang, H. Ren, W. Li, *Front. Chem.,* **11**, 1093435 (2023). 10.3389/fchem.2023.109343
10. A. Lassin, C. Christov, L. André, M. Azaroual, *Amer. J. Sci.,***315**, 204 (2015). DOI: 10.2475/03.2015.02
11. A. Lassin, L. André, *J. Chem. Thermodyn.,* **176,** 1 (106927). (2023). doi.org/10.1016/j.jct.2022.106927
12. N. Greenfield, Lithium Mining Is Leaving Chile's Indigenous Communities High and Dry (Literally) (2022). https://www.nrdc.org/stories/lithium-mining-leaving-chiles-indigenous-communities-high-and-dry-literally.
13. V. Marcinov, J. Klimko, Z. Takáčová, J. Pirošková, A. Miškufová, M. Sommerfeld, C. Dertmann, B. Friedrich, D. Oráč, *Metals,* **13**, 1213 (2023). https://doi.org/10.3390/met13071213.
14. A. Zdanovskii, E. Soloveva, E. Liahovskaia, N. Shestakov, P. Shleimovich, L. Abutkova, L. Cheremnih, T. Kulikova, Experimentalnie dannie po rastvorimosti*,* vols. I-1, I-2, II-1 and II-2, Khimizdat, St. Petersburg, 2003.
15. C. Christov, *J. Chem. Thermodyn.*, **32,** 285 (2000) https://doi.org/10.1006/jcht.1999.0564
16. S. Donchev, I. Ismailov, I. Parushev, C. Christov, *Res. J. Pharm. Biol. Chem. Sci.* (*RJPBCS*) **10** (5), 83 (2019) https://doi.org/10.33887/rjpbcs/2019.10.5.12
17. G. Schwarzenbach, H. Flashka, Komplexometrische Titration (in Russian), Izd. Khimiya, Moscow, 1970.
18. F. Schreinemakers, *Z. Physik. Chem.,* **11**, 75 (1893) (see also refs. 1, 2, 15, and 16).
19. A. Kirgintsev, L. Trushnikova, V. Lavrentieva, Solubility of inorganic compounds in water, Izd. Khimiya, St. Petersburg, 1972.

Bulgarian Chemical Communications, Volume 57, Issue 1 (pp. 32-36) 2025 *DOI: 10.34049/bcc.57.1.5682*

An efficient and economical approach to hydrogen peroxide detection and neutralization utilizing molybdenum sensors

Ch. Douvris[1*], D. Bussan[2]

[1] *Department of Biological and Chemical Sciences, New York Institute of Technology, Theobald Science Center, Old Westbury, NY 11568*
[2] *Derek Bussan's Consulting LLC, Durango, Iowa 52039*

Received: November 20, 2024; Revised: February 10, 2025

Considering that significant challenges associated with the detection of peroxide-based explosives such as TATP and HMTD, as well as the fact that hydrogen peroxide (H_2O_2) is both a synthetic precursor and a degradation product of them, this study presents a rapid, cost-effective, and environmentally friendly approach for detecting and neutralizing H_2O_2 using Mo-based sensing devices. The method exploits the color change of a particular Mo compound, $Mo_2O_5(OH)$, from blue to pale yellow upon reaction with H_2O_2, due to formation of MoO_3. For this work, butanol bronze-based test strips coated with Mo w

ere created and exposed to various concentrations of H_2O_2. The color change was monitored using a camera and analyzed with ImageJ software. The reaction was found to follow a first-order kinetics, with the rate of color change proportional to the concentration of H_2O_2. The slope of the phenomenological rate *versus* H_2O_2 concentration was found to be 16.752 color change % s^{-1}. The results demonstrate the high potential of Mo bronze-based test strips for low-cost detection and neutralization of H_2O_2, offering a promising solution to the challenges posed by related dangerous explosives.

Keywords: Molybdenum, Hydrogen peroxide, Sensing devices

INTRODUCTION

The global rise in terrorist activities involving explosive devices has created an urgent need for effective methods to detect and neutralize these instruments [1]. Explosives, whether solid or liquid, exist in a metastable state, enabling rapid chemical reactions without external reactants such as oxygen. Peroxide-based explosives, particularly triacetone triperoxide (TATP) and hexamethylene triperoxide diamine (HMTD), have gained prominence due to their extensive use by terrorist organizations in the manufacturing of improvised explosive devices [13]. These cyclic peroxides pose a challenge for standard explosive detectors as they lack nitrogen-containing functional groups, making their identification difficult [2]. Unfortunately, peroxide-based explosives like TATP and HMTD continue to be used in numerous terrorist attacks, and attempts have been made to smuggle their precursor materials onto aircraft for in-flight bomb production [2, 3].

Hydrogen peroxide (H_2O_2) has found widespread industrial uses and applications and due to its property of being unstable and undergoing disproportionation, it is also used as a precursor for the synthesis of the aforementioned homemade explosives (TATP, HMTD), as well as several others and it is listed under peroxide-based energetic materials [4–9]. In view of this, it is generally accepted that H_2O_2 is a significant compound for determination of peroxide-based explosives [10–13]. As a result of the importance for improved detection methods that extend beyond traditional contexts and in particular the need for determining traces of H_2O_2, we present a rapid, cost-effective, and environmentally friendly approach for detecting and neutralizing it, using Mo sensing devices [14]. The choice of the Mo materials was due to selectivity, stability and intense color of its acompounds and the precedent of its applications in colorimetric detection of various species in solutions [10–13, 15]. Exploiting the reaction shown in equation (1), in which the original blue color of a Mo compound, $Mo_2O_5(OH)$, with a metal charge transfer band at 710 nm, changes to a pale-yellow color (MoO_3) due to its reaction with H_2O_2, we designed Mo butanol bronze-based coated test strips and exposed them to various concentrations of H_2O_2

$$2Mo_2O_5(OH) + H_2O_2 \rightarrow 4MoO_3 + 2H_2O \quad (1)$$

The resulting color change was monitored using a camera to allow for the determination of the reaction kinetics and in particular how the rate of

* To whom all correspondence should be sent:
E-mail: cdouvris@nyit.edu

color change may be related to the concentration of H_2O_2.

MATERIALS AND METHODS

All chemicals used in the experiment were of reagent grade (ACS reagent grade) and were employed without additional purification. UV spectrophotometric analysis was carried out using a Carey 50 UV-VIS spectrophotometer. Images of the test strips during exposure to H_2O_2 were captured using a Logitech Pro 9000 USB camera, and photographs were taken at 15 cm distance from the surface. An open-source software (ImageJ), provided by the National Institute of Health was used to perform image analysis to process the kinetic data. Butanol bronze was synthesized following the catalytic procedure outlined in the literature [16]. Test strips were prepared using a VWR ergonomic high-performance pipette, ranging from 0.5 μL to 10.0 μL. Subsequently, 3.15 μL of butanol bronze ink was applied to each test strip pad. This quantity was determined to be sufficient to completely saturate each individual test strip. Camera settings were adjusted according to the room's lighting conditions, and the optimal settings for the specific room used in the experiments are detailed in Table 1.

Table 1. Camera settings

Settings	Values
Brightness	179
Contrast	35
Saturation	50
Sharpness	224
Backlight compensation	1
Focus	175
LED mode	3

The test strips were then cut to length, fitted to a weigh boat, and taped down, in order so that the test strip would be stable through the whole video recording process. A photo of a test strip that is ready to be used for testing hydrogen peroxide is given in Figure 1.

Four different concentrations of H_2O_2 were used in the experiment with each concentration having three runs, with a total of 12 runs. A commercially available solution of 30% H_2O_2 was diluted to prepare the following concentrations 0.0206%, 0.0846%, 0.1208% and 0.333%. The concentrations were determined *via* separate iodometric titrations using a sodium thiosulfate solution. The prepared solutions were analyzed, and their concentrations were verified to be within a 1% deviation from the nominal value. After the test strip was put underneath the camera and the correct camera settings were utilized, H_2O_2 was poured onto the test strip and the camera recorded the test strip changing colors. The recording showed that the test strip pad turned white, as demonstrated in Figure 2.

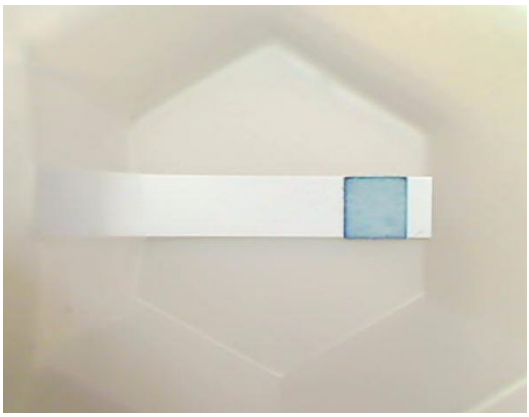

Figure 1. Unreacted butanol bronze test strip.

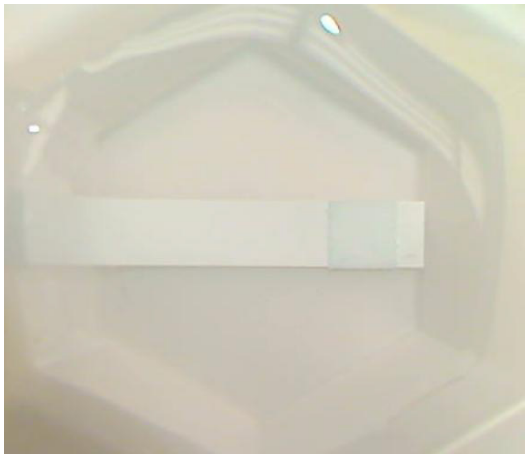

Figure 2. Butanol bronze test strip after reaction with H_2O_2.

Once H_2O_2 was poured, an image of the test strip was captured and saved every 30 s by a Python script using the OpenCV software package. To ensure consistent image capture, a workaround was implemented where the camera was read three times, and the last image was selected for analysis.

RESULTS AND DISCUSSION

In this study, a Mo butanol bronze-based ink was synthesized for the purpose of detecting and neutralizing H_2O_2. As previously reported, the blue colored solid $Mo_2O_5(OH)$ reacts swiftly with both H_2O_2 solutions and organic peroxides, resulting in the formation of MoO_3 and water (equation 1) [17].

Previous studies have demonstrated that XploSafe PS test strips are an effective tool for

measuring peroxide concentrations in solution. These test strips are specifically engineered to quantify peroxide levels when immersed in peroxide-containing solutions [18]. For our experiments, each test strip was mixed with a set of standard H_2O_2 solutions of the following concentrations: 0.0206%, 0.0846%, 0.1208% and 0.333%. Upon mixing, the test strip underwent a color change from blue to pale-yellow, with the final color intensity exhibiting an inverse relationship to the solution concentration. This observation was confirmed by plotting the natural logarithm of the normalized intensity *versus* exposure time which is shown in Figure 3 for the concentration 0.0206%, while Figure 4 shows the color intensity over time. For the other three concentrations the corresponding data were collected.

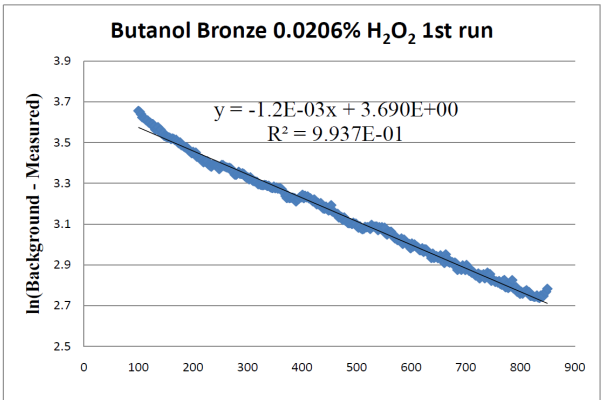

Figure 3. The natural logarithm of normalized reflected intensity with time from an XploSafe PS test-strip during the peroxide exposure to H_2O_2 at a concentration of 0.0206%.

After removing the test strip from the solution and shaking off the excess liquid, an image of the test strip was captured within a 10-min timeframe. Stability tests revealed that the color remained consistent for a minimum of 24 h under standard laboratory conditions. Images of each test strip were acquired using a single-lens reflex camera. The captured images were then processed using ImageJ software, where each color channel was separated and averaged over the test strip pad area. Exposure to H_2O_2 caused the XploSafe PS test strips to change color from blue to pale-yellow. This color change is attributed to the absorption of light by the test strips upon reacting with H_2O_2, resulting in reduced light reflection.

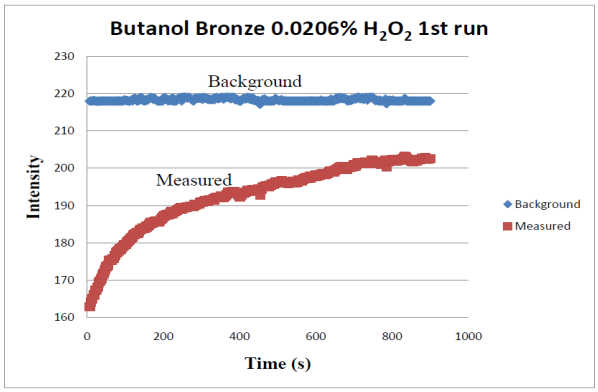

Figure 4. Butanol bronze 0.0206% H_2O_2 first run.

The observed color changes were consistent with the color scale provided by Xplosafe. The described setup for optical measurement of the test strip response offers a significantly more accurate quantification of the H_2O_2 concentration in the solution compared to the visual comparison of the test strip with a color chart. The intensity of the reflected light is proportional to the concentration of the molybdenum compound. A control experiment using a blank test strip showed no observable color change upon exposure to H_2O_2.

Linear regression analysis was performed on the data points between 80% and 20% of the maximum intensity. All fitted lines exhibited an R^2 value greater than 0.90. The negative slope obtained from the linear regression represents a phenomenological first-order rate constant. At later time points, the decrease in reflected intensity decelerates and eventually ceases when all the accessible Mo complex has been consumed. The linear fit suggests that the color development is limited by the H_2O_2 concentration, and the reaction between H_2O_2 and the Mo species occurs rapidly on the time scale of this experiment.

The response of the test strips to varying H_2O_2 concentrations can be quantified by plotting the rate constant as a function of concentration. Each phenomenological first-order rate constant represents the rate of color change over time at a given percentage. This rate is proportional to the fixed concentration of Mo species at each percentage. Therefore, the measurement represents the rate of color change per given percentage over time. Plotting the results against the percentage yields the color change per ppm per second. The linear relationship is illustrated in Figure 5 with the slope of the line determined to be 16.752 color change % s^{-1}. This result is comparable to the value reported for a titanium complex previously studied in our laboratory using similar methods [18].

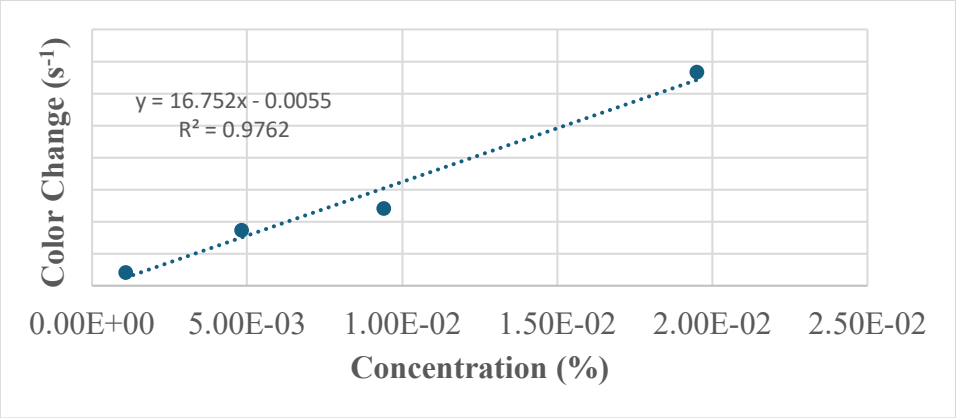

Figure 5. The phenomenological rate *versus* hydrogen peroxide concentration in ppm.

The results of this study demonstrate that Mo bronze-based test strips offer a rapid and cost-effective approach for detecting hydrogen peroxide in liquid solutions, with a detection limit estimated to be in the range of 0.09 to 0.18 ppm. This performance is comparable to, and in some cases exceeds, that of previously reported methods. For instance, titanium (IV)-based test strips, as described by Hossain *et al*. (2022) [18], achieve a detection limit of 1 ppm for gas-phase hydrogen peroxide with a 1-min exposure and 0.01 ppm with a 1-h exposure [18]. While the Ti-based method excels in gas-phase detection, the Mo-based test strips presented here are particularly well-suited for liquid-phase applications, such as the detection of peroxide-based explosives, where rapid and sensitive detection is critical. Both methods exhibit first-order kinetics, with the rate of color change proportional to the H_2O_2 concentration, indicating that the underlying chemical reactions are similarly efficient and robust. The primary advantage of the Mo-based test strips lies in their simplicity and environmental friendliness, making them ideal for field applications where cost and ease of use are paramount. In contrast, the Ti-based method requires careful selection of light sources and filters to avoid color leakage issues, which can complicate its deployment in certain settings. However, the Ti-based method's ability to detect H_2O_2 in both liquid and gas phases, provides a broader range of applications, particularly in industrial environments where monitoring airborne H_2O_2 is essential. Future work could explore extending the Mo-based method to gas-phase detection, potentially combining the strengths of both approaches to create a versatile and highly sensitive detection system for hydrogen peroxide in various contexts.

The detection limit for the Mo bronze-based test strips was estimated using a signal-to-noise ratio (S/N) approach, where the detection limit is defined as the lowest concentration of H_2O_2 that can be reliably detected. This was calculated using the formula:

$$\text{Detection Limit (DL)} = \frac{3 \times \sigma}{\text{Sensitivity}}$$

where σ represents the standard deviation of the noise (background signal), and the sensitivity is given by the slope of the phenomenological rate *versus* H_2O_2 concentration plot, which was determined to be 16.752 color change % s^{-1}. Assuming a conservative noise level (σ) of 1% of the maximum reflected intensity, the detection limit was estimated to be approximately 0.179 ppm. This value could be further refined with access to the raw background signal data; for example, if the noise level were reduced to 0.5%, the detection limit would improve to 0.0895 ppm. These results demonstrate the high sensitivity of the Mo bronze-based test strips for detecting low concentrations of H_2O_2, making them a promising tool for applications such as the detection of peroxide-based explosives. The estimated detection limit is competitive with previously reported methods, such as titanium (IV)-based test strips, which achieve a detection limit of 1 ppm for gas-phase H_2O_2 with a 1-min exposure and 0.01 ppm with a 1-h exposure. This highlights the potential of the Mo-based method for liquid-phase detection, particularly in scenarios where rapid and cost-effective monitoring is required.

CONCLUSION

This study demonstrates that the combination of Mo bronze-ink based test strip with a regular camera can quantify H_2O_2 with high sensitivity. The exposure of Mo bronze to H_2O_2 leads to the development of a characteristic intense yellow color. The test strips were tested with concentrations between 0.0206-0.3330%. The reaction was completed fast, and a first-order behavior in the color

change with exposure time was observed, implying that the reaction between the Mo complex in the test strips with H_2O_2 is rapid on the time scale of these experiments. The change in intensity is linearly proportional to the concentration of H_2O_2 with the resulting color change being 16.752 % s^{-1}. As a result, Mo bronze-based test strips have high potential for low-cost detection of H_2O_2-containing devices which could include peroxide-based explosives.

REFERENCES

1. R. Meyer, Explosives, Verlag Chemie, 1977.
2. J. Oxley, J. Smith, Peroxide Explosives, in: Detection and Disposal of Improvised Explosives, Springer, 2006, p. 113.
3. C. Denekamp, L. Gottlieb, T. Tamiri, A. Tsoglin, R. Shilav, M. Kapon, *Organic Letters,* **7**, 2461 (2005).
4. K. N. Barber, Novel Environmental and Explosives Detection Applications for Molybdenum Oxides, Oklahoma State University, 2009.
5. W. R. Sanderson, *Pure and Applied Chemistry, 7***2**, 1289 (2000).
6. G. Rarata, J. Smętek, *Materiały Wysokoenergetyczne*, **8**, 56 (2016).
7. B. Stiasny, Investigation of organic peroxides and their properties as energetic materials, 2016.
8. E. Espinosa-Fuentes, A. Peña-Quevedo, L. Pacheco-Londoño, R. Infante-Castillo, S. Hernández-Rivera, Explosive Materials: Classification, Composition and Properties; Chemical Engineering Methods and Technology, Series 259, 2011.
9. A. Wahab, C. Douvris, J. Klima, F. Šembera, J. Ugolotti, J. Kaleta, J. Ludvik, J. Michl, *Inorganic Chemistry,* **56**, 269 (2017).
10. A. Üzer, S. Durmazel, E. Erçağ, R. Apak, *Sensors and Actuators B: Chemical,* **247**, 98, 2017.
11. C. Yang, Z. Xie, H. Zhang, H. Li, Y. Cai, J. Wang, J. Du, H. Yu, Y. He, *ACS Sustainable Chemistry & Engineering*, **7**, 18985 (2019).
12. C. Lampropoulos, G. Rashad, C. Douvris, *Molecules***, 26**, 6838 (2021).
13. R. Li, H. An, W. Huang, Y. He, *Sensors and Actuators B: Chemical*, **259**, 59 (2018).
14. J. R. Ingham, G. L. Donati, L. Douvris, G. Bartzas, D. D. Bussan, C. Douvris, *Science of The Total Environment,* **930**, 172790 (2024).
15. D. D. Bussan, Applications of Molybdenum Utilized in Sensing Devices, Oklahoma State University, 2011.
16. G. A. Buttigieg, A. K. Knight, S. Denson, C. Pommier, M. B. Denton, *Forensic Science International*, **135**, 53 (2003).
17. A. W. Apblett, M. Chehbouni, L. E. Reinhardt, *Ceramic Transactions,* **174**, 39 (2012).
18. R. Hossain, J. J. Dickinson, A. Apblett, N. F. Materer, *Sensors,* **22**, 6635 (2022).

Bulgarian Chemical Communications, Volume 57, Issue 1 (pp. 37-39) 2025 *DOI: 10.34049/bcc.57.1.5685*

The theory for the disperse structure of real crystals by Dimiter Balarew, as a predecessor of the nonclassical crystallization of mesocrystals

Chr. Balarew*

Institute of General and Inorganic Chemistry, Bulgarian Academy of Sciences,1113 Sofia, Bulgaria

Received: December 03, 2024; Accepted: December 27, 2024

The generally accepted classical theory of crystal growth, developed by Kossel and Stranski at the end of the 1920s, describes crystallization as a layer-wise deposition of atoms, ions or molecules on the surface of a crystal nucleus. At the same time, Dimiter Balarew developed the idea for colloid chemical growth of real crystals from salt solutions, which consists of aggregation of clusters sized about 0.01 μm (nanoparticles) into a disperse structure of real crystals. For many reasons, this theory remained in forgetfulness. However, in the last three decades an increasing number of examples were observed which could not be explained by the classical models. Finally, it was proven that the crystals can also grow by attachment of nanoparticles, a process known as nonclassical crystallization. So, Dimiter Balarew was perhaps the first scientist who raised the idea of self-organized agglomeration through oriented attachment of nanoparticles in salt solutions and formation of crystals with a disperse structure.

Keywords: Crystal growth, Nonclassical crystallization, Nanoparticles, Mesocrystals.

More than 80 years ago Dimiter Balarew created his theory of real crystal growth from salt solutions. On the basis of his experimental data accumulated in the 1930s, he launched the idea for colloid chemical growth of real crystals from salt solutions, resulting in a dispersed structure of the real crystals. In 1939 he summarized the data and published the monograph "The disperse structure of the solid systems" [1].

However, at that time the classical theory of crystal growth developed by Gibbs [2], Volmer and Weber [3], Kossel [4] and Stranski [5] was generally accepted. The classical theory describes crystallization as an adsorption process of atoms, ions or molecules on the surface of a crystal nucleus and their subsequent migration over the crystal surface until they reach edges and kinks where their attachment is energetically favorable (Fig. 1a). In this way, a layer-by-layer crystal growth is achieved.

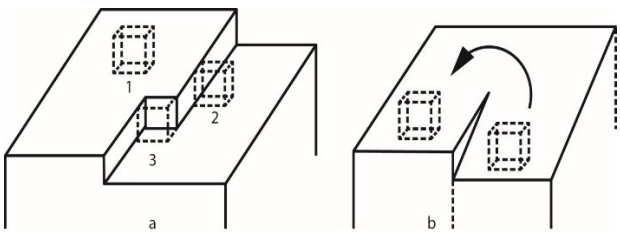

Figure 1. Crystal growth: (a) Molecular-kinetic theory of Kossel-Stranski [4, 5]; (b) Screw dislocations mechanism [6].

Burton *et al.* later developed a crystal growth model through screw dislocations and spiral growth (Fig. 1b) [6].

Considering the classical models of crystal growth by successive deposition of individual ions, atoms or molecules on the surface of a growing crystal, it is obvious that these models cannot be valid for the cases of salts crystallization from aqueous solutions. In aqueous solutions of salts free ions do not exist. The ions are always hydrated, forming ion pairs and complexes with each other. The latter are grouped into associates of different sizes depending on the composition of the solutions, the concentrations of the salts and the temperature.

According to the classical theories nucleation is considered to take place in a supersaturated solution by stochastic solute clustering. The earliest crystal precursor is considered to be a cluster of critical size [3]. Recently, it was shown that stable clusters play a dominant role in the prenucleation stage [7]. This means that nucleation is not a problem of critical size only, it can be speculated that entropic solvent effects intervene as well. It follows that the lowest critical supersaturation needed for nucleation is expected for those salts whose solutions contain sufficiently high concentration of complexes having crystal structure analogous with fragments from the structure of the crystallizing salt [8].

* To whom all correspondence should be sent:
E-mail: *balarew1@gmail.com*

Dimiter Balarew developed the idea for a colloid chemical growth of real crystals through agglomeration of particles sized about 0.01μm, which he called elementary crystals (i.e., nanoparticles according to modern terminology). The latter, almost equally oriented (self-organized), being three-dimensionally arranged, aggregate into a disperse structure of a real crystal [1]. On Figure 2, Dimiter Balarew showed the attachment of the elementary crystals for the formation of the real crystal on the example of $BaSO_4$.

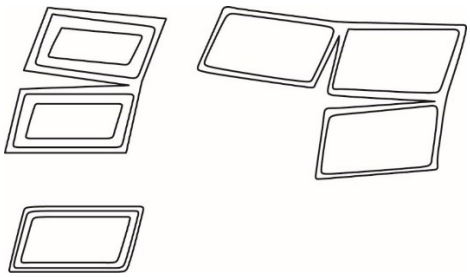

Figure 2. Attachment of the elementary crystals of $BaSO_4$ during the formation of the real crystal [1].

On Figure 3 he showed the morphology of crystals with well-formed faces, edges and corners (Fig. 3a), dendritic crystals (Fig. 3b) and amorphous particles (Fig. 3c), all of them obtained through attachment of the elementary crystals at different kinetics of crystallization: slow crystallization yields well-shaped crystals (a), faster crystallization yields dendritic crystals (b) while amorphous particles (c) are obtained under fast crystallization.

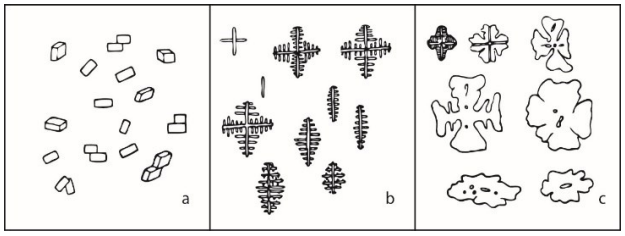

Figure 3. Structures obtained through attachment of the elementary crystals at different kinetics of crystallization: (a) Crystals with well-formed faces, edges and corners; (b) Dendritic crystals; (c) Amorphous particles [1].

Both the oriented self-organization of the elementary crystals and their subsequent attachment are due to the following specific physicochemical properties of the elementary crystals:

- the high values of their surface-to-bulk ratio;
- their fine building composition differing from the stoichiometric one and the different characteristics of the faces, edges and corners of the elementary crystals;
- their ability for ordering in common crystallographic orientations and aggregation as a result of electrostatic and anisotropic van der Waals forces.

By the term "fine building composition of the crystals" Dimiter Balarew implies crystals with a composition different from the stoichiometric. So, if we suppose, for instance, that we have a CaF_2 crystal with the dimensions of a crystallographic unit cell, it consists of 14 Ca^{2+} ions and 8 F^- ions, i.e., the Ca/F ratio is 1.75 (Figure 4).

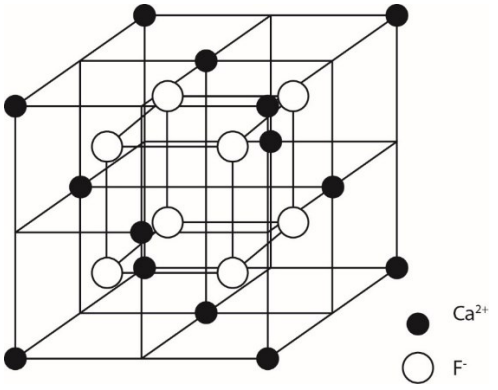

Figure 4. Unit cell of the CaF_2 structure (Ca/F ratio = 1.75) [1].

As the size of this crystal increases, the Ca/F ratio decreases, as shown in Figure 5, and at a sufficiently large crystal size it reaches the stoichiometric composition. This range of crystal sizes actually corresponds to nanoparticle-sized crystals.

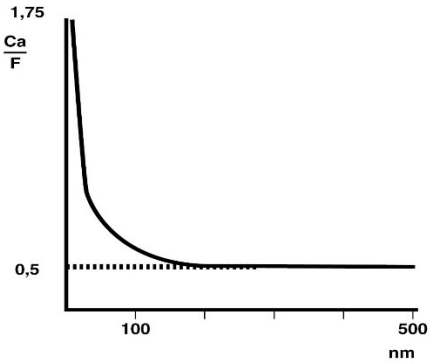

Figure 5. Dependence of the composition of the crystals on their size as numbers of the unit cells [1].

Through formation of the actual crystals by aggregation of the nanocrystals, internal surfaces remain in the bulk of the macrocrystal, which are hydrated, also containing adsorbed admixtures from the mother liquid. Dimiter Balarew called this occurrence "an internal adsorption process".

The theory of Dimiter Balarew remained more or less in forgetfulness. However, in the last three decades an increasing number of examples were observed, which could not be explained by classical models. Finally, it was proven that a crystal can grow

not only by attachment of atoms, ions or molecules, as in the classical models but also by attachment of particles, a process known as nonclassical crystallization. The idea for the occurrence of a self-assembly process of agglomeration of nanoparticles as a structure-generating process of formation of macrocrystals, close to the idea developed by Dimiter Balarew, was created in the early 2000s by Cölfen and Antonetti [9] who named the crystals obtained according to this mechanism mesocrystals (shortened name for mesoscopically structured crystals). Cölfen defined the mesocrystals as superstructures composed of nanoparticles, being arranged three-dimensionally in crystallographic register. Mesocrystals are often only intermediate structures in a nonclassical crystallization pathway leading to a final single crystal by nanoparticle fusion [10].

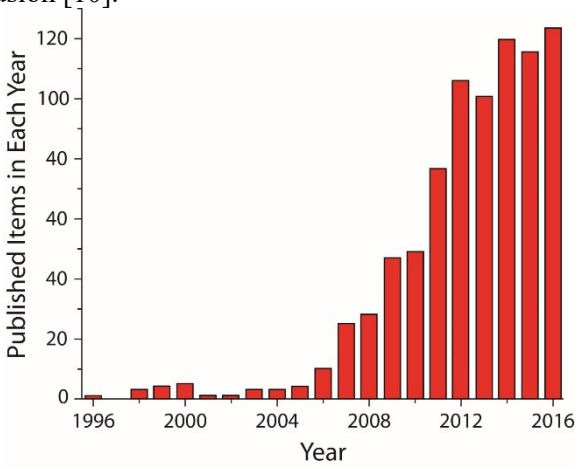

Figure 6. Papers published per year on mesocrystals as numbered by Sturm *et al.* [12] by the search of word *mesocrystal* in the Web of Science by the end of 2016.

Since mesocrystals have high crystallinity, as well as high porosity, they are promising substitutes for single-crystalline and/or porous polycrystalline materials in many applications such as catalysis, sensing, and solar-energy conversion [11]. Figure 6 shows the growing interest in mesocrystals in the years 1996 - 2016 [12].

REFERENCES

1. D. Balarew, Der disperse Bau der festen Systeme, Verlag Th. Steinkopf, Dresden u. Leipzig, 1939.
2. J. W. Gibbs, *Trans. Comm. Acad. Arts Sci.,* **3**, 108 (1876).
3. M. Volmer, A. Weber, *Zeitschr. für physik. Chemie,* **119**, 277 (1926).
4. W. Kossel, *Nachr. Götting. Ges.,*135 (1927).
5. I. N. Stranski, *Zeitschr. für physik. Chemie – Stöchiometrie u. Verwandtschaftslehre,* **136,** 259 (1928).
6. W. K. Burton, N. Cabrera, F. C. Frank, *Phil. Trans. Royal Soc. London,* **243**, 299 (1951).
7. D. Gebauer, H. Cölfen, *Nano Today,* **6**, 564 (2011).
8. Chr. Balarew, S. Tepavitcharova, D. Rabadjieva, S. Kamburov, *Pure Appl. Chem*., **87**, 445 (2015).
9. H. Cölfen, M. Antonetti, Mesocrystals and Nonclassical Crystallization, Wiley & Sons, USA, 2008.
10. H. Cölfen, Handbook of Biomineralization: Biomimetic and Bioinspired Chemistry, P. Behrens, E. Bäuerlein (eds.), Wiley-VCH, Weinheim, 2007, p. 39.
11. L. Zhou, P. O'Brien, *J. Phys. Chem. Lett.*, **3**, 620 (2012).
12. E.V. Sturm (née Rosseeva), H. Cölfen, *Crystals,* **7**, 207 (2017).

Bulgarian Chemical Communications, Volume 57, Issue 1 (pp. 40-46) 2025 *DOI: 10.34049/bcc.57.1.5680*

Energy-efficient enrichment of bioslurry and methane content of biogas from wheat flour in a bio-electrochemical anaerobic digester

H. M. Jariwala[1], Y. C. Rotliwala[2*]

[1]*Research scholar, Chemical Engineering Department, Government Engineering College, Valsad, Gujarat Technological University, Ahmedabad 382424, India*
[2]*Chemical Engineering Department, Pacific School of Engineering, Surat, Gujarat Technological University, Ahmedabad 382424, India*

Received: November 12, 2024; Revised: February 11, 2025

The methane-rich biogas resulting from an anaerobic digester (AD) was utilized as a potential source of energy, whereas the bioslurry, due to its rich nutrients content, was explored as a fertilizer. The effect of a bio-electrochemical system (BES) integrated with a conventional anaerobic digester (AD) for biogas enrichment is widely reported. This paper presents a comparative study of the characteristics of bioslurry resulting from two different digestors, i.e., only-AD and AD-BES. In contrast to only-AD, AD-BES-derived bioslurry showed a significant increase in nitrogen, phosphorus and potassium content to the tune of 14.29%, 37.04% and 19.26%, respectively. Moreover, it showed an increment in pH and reduction of total solid, volatile solid, C:N ratio. This paper also includes a comparison of two different methods for analyzing methane and carbon dioxide concentration in the biogas, i.e., statistical analysis-based method using ORSAT apparatus and gas chromatographic (GC) method. The comparison showed little difference in methane and carbon dioxide concentrations between the two methods (1.66 % and 2.79%, respectively). The comparison of the energy requirement (kWh) of AD-BES and of other methane-enriching conventional methods demonstrated a noteworthy reduction in energy requirement of AD-BES (43-90%). The results showed that AD-BES provides significantly enriched nutrients of bioslurry, and increased the concentration of methane in the biogas at lower energy requirement.

Keywords: Anaerobic digester, BES (bio-electrochemical system), bio-fertilizer, digestate (bioslurry), enrichment

INTRODUCTION

In order to improve crop productivity and maintain soil fertility, frequent uses of chemical fertilizers and pesticides become common practices in agriculture fields leading to harmful effects on human health and also cause various environmental issues. In India, application of nitrogenous chemical fertilizers becomes the costlier affair due to increasing price of raw materials (petroleum) for chemical fertilizers production. Under the circumstances, it is creating a large gap of actual supply for supplementing nitrogenous fertilizer as a nutrient to plant growth [1]. Thus, conventional practices demand replacement in farming methods through the use of sustainable approaches. Presently, organic farming as a sustainable agriculture practice has gained global attention. In the year 2022, a FiBL (Institute of Organic Agricultural Research) survey reported that India ranked first in numbers of organic farmers (about 25 lakh), which increased by 93 percent as compared to year 2021 after Uganda (4 lakh) and Thailand (about 2 lakh). Despite numerous advantages of organic farming practice, poor crop productivity and high cost of production limits its acceptability as a routine farming practice [2].

In terms of resource recovery from biowaste, anaerobic digestor is considered to be a clean, efficient and sustainable technique for generation of energy from organic wastes (dung, cattle waste, food waste, agriculture waste and municipal solid waste) [3]. The products of the anaerobic digestor mainly consist of methane-enriched gas known as biogas utilized as a domestic cooking fuel/commercial fuel (compressed natural gas) and residual slurry known as bioslurry [4]. The bioslurry, originating from high-solid content waste materials, is a complex mixture composed of various dissolved organic matters, salts, microbes, and other suspended solids (SS) [5, 6]. It contains nutrients such as nitrogen (N), phosphorus (P), potassium (K), and other important elements for plant growth, which are utilized for soil quality improvement and crop yield [4, 7, 8]. Also, the bioslurry is reported to be creating a closed-loop system where nutrients are recycled from biowaste creating zero waste valorization of residues to accomplished circular economy and reduced environmental impacts [9, 10]. A significant improvement in crop yield of soybean, sunflower, wheat, rice and sweet corn is reported using bioslurry on agricultural fields [9, 11-13].

* To whom all correspondence should be sent:
E-mail: *yrotliwala@yahoo.com*

The utilization of bioslurry as an effective soil conditioner is widely reported. The high water content (~93%) in the bioslurry imparts bulkiness and raises handling challenges [14-16]. Also, some of the authors demonstrated that the anaerobic digestion favors phosphorous precipitation leading to increased pH of the resulting bioslurry [17, 18]. Moreover, few studies reported that alkaline pH encourages loss of nitrogen in the form of volatile ammonia. Due to the typical nature of alkaline pH of bioslurry [19,20], transformation rate of C/N decreases. Thus, application of bioslurry in its present form limits its uses as a bio fertilizer at agricultural fields and demands further enrichment and quality improvement in bioslurry. To the best of our knowledge, very few studies (mainly on mechanically dried slurry) are reported in terms of bioslurry enrichment. Thus, the idea came to look for alternative methods for enrichment of bioslurry through AD-BES using wheat flour (carbohydrate - 82%, protein - 14% and fat - 4%) as a substrate. The application of AD-BES for enrichment of bio slurry is not yet reported.

Our previous study [21] revealed that integration of BES with an AD digester improves volume and quality (methane- enrichment) of the resulting biogas. It showed that BES-integrated AD increases the volume of biogas by 66.7% and the concentration of CH_4 in raw biogas by 81.5 v/v% (from 64 v/v% CH_4) at a supplied voltage of 0.3 V. Further, in our previous study a statistical analysis-based method using ORSAT apparatus was used for the determination of CO_2 and CH_4 in biogas. This paper presents a comparative study of bioslurry characteristics (mainly N, P and K) resulting from only-AD and AD-BES. This paper also includes a comparison of two different methods, i.e., statistical analysis-based ORSAT apparatus (reported in earlier publication) and gas chromatography (GC) for analyzing the concentration of methane in the biogas. Besides, a comparative study of the energy requirements for the operation of AD-BES and other conventional method of methane enrichment is addressed.

MATERIALS AND METHODS

Feedstock

Cow dung was used as an inoculum with wheat flour substrate-to-water ratio of 1:1 (by weight). A 20 kg homogeneous mixture of inoculum was created by combining equal weights of cow dung and water. This mixture was tested for total solids (TS) and volatile solids (VS), resulting in measurements of 10% and 7.5%, respectively [21]. After starting biogas generation within 4 to 5 days, substrate was added at a frequency rate of 3 g per day for the duration of 25 days.

Digester setup

As shown in Figure 1, the digester has two cylindrical floating domes fabricated with high-density polyethylene (HDPE); two digesters (only-AD and AD-BES) of 20 L capacity were used to carry out experimental runs at 30°C ± 5°C for the duration of 25 days. Conventional Only-AD digester was without electrodes, whereas the AD-BES digester included two carbon (99.9% pure graphite, length - 127 mm, diameter -25.4 mm, surface area - 11147.56 mm^2) electrodes (anode and cathode) installed at the bottom at a distance of 210 mm. A DC power supply to regulate the voltage (Tektronix, PWS2185, 0-18 V, 5A, India) was installed across these two electrodes. Detailed drawing of the AD-BES digester along with all accessories and specifications (high-density polyethylene (HDPE, cylindrically shaped floating dome type (capacity 20 L)) can be found in our earlier publication [21].

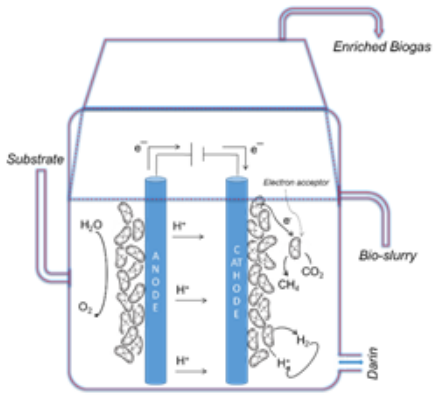

Figure 1. Schematic diagram of a bio-electrochemical integrated anaerobic digester

Procedure

The overflow of the bioslurry (supernatant) was obtained at an interval of 5 days from the drain line installed at the outer side of the digester. In order to remove solids from the bioslurry, it was filtered out through Whatman-597 (30 µm) filter paper and further utilized for characterization. The resulting biogas from anaerobic digesters was collected from a sampling line fitted at the top of the floating dome and analyzed in a gas chromatograph (GC).

Determination of energy supply to digester

The energy requirement of AD-BES digester was calculated in kwh for the total run time of 25 days at 30 °C ± 5 °C (laboratory operating condition). Figure 2 shows the representative circuit diagram of the

AD-BES digester. A DC power supply regulator was used to regulate the supplied voltage across the electrodes. The experimental runs were conducted in an AD-BES digester at a supplied range of voltage 0.1 V to 1.5 V. The current was measured using A-meter attached with digester. The measured current was in the range of 0.0095 A to 0.095 A. The energy supplied was calculated using equation 1:

$$E_{kwh} = \frac{V_V \times \mathrm{I_A} \times t_h}{1000} \quad \ldots (1)$$

where, E_{kwh}= energy supplied in kwh, V= voltage supplied, volt, I = current generated, ampere, t = duration of energy supply, h.

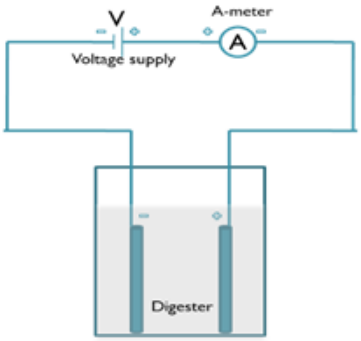

Figure 2. Circuit diagram of AD-BES digester

Determination of biogas slurry and biogas

The Soil Science Department, Navsari Agriculture University, Gujarat, India kindly supported for the characterization of N, P and K of bioslurry. The modified Kjeldahl's method (IS 3025 (Part-34) 2019) was used for nitrogen determination in the bioslurry. Phosphorus (P) content was determined after wet digestion [22]. Flame photometry (IS 3025 (Part 45) 2019) was adopted for potassium measurement in the bioslurry [22, 23]. The pH was measured with pH meter (LABMAN LMPH-10, India). Total solids (TS) and volatile solids (VS) were determined by the standard method (APHA 2540, 2012). CHN elemental analyzer (Leco CHN 2000) was used to measure total organic carbon and nitrogen (C/N) [24].

In our previous study, ORSAT apparatus was used for statistical analysis-based determination of CO_2 and CH_4 in biogas [21]. In order to compare the results of the statistical method, this paper addressed the determination of CO_2 and CH_4 in biogas using gas chromatographic analysis carried out at the Quality Control Laboratory, BEIL Infrastructure Ltd., Ankleshwer, India. Biogas produced from only-AD and AD-BES was collected in gas bladders and analyzed through Shimadzu (GC 2010 plus) GC equipped with an FID detector and a capillary column (DC -10, 25 m × 0.32 mm × 0.5 µm (detector film thickness)). The temperatures of the column chamber, inlet chamber and detector were maintained at 40 ^{0}C, 60 ^{0}C and 180 ^{0}C, respectively. The carrier gas, high purity nitrogen, was used at a flow-rate of 3 ml/min. The flow-rate of the sample was 30 ml/min, maintained injection volume was 1 µl at total run time of 10 min. The split ratio of gas sample in the inlet chamber was 1:1.15. The area under the curve 20520 was considered for standard methane of 250 mg/L.

RESULTS AND DISCUSSION

Characterization of the biogas

Figures 3 (a) and (b) show the chromatograms of biogas samples derived from AD and AD-BES, respectively. The peak areas of the tested biogas profiles were used to determine biogas composition. The chromatogram of only-AD showed methane and carbon dioxide peak area of 55383193 ppm and 5490952 ppm at retention time of 3.883 min and 4.588 min, respectively. As shown in chromatogram, in contrast to only-AD, AD-BES digester derived biogas indicated higher peak area of methane gas, i.e. 68194099 ppm and lesser peak area for carbon dioxide gas, i.e. 3802695 ppm. In order to determine the concentration of methane and carbon dioxide in biogas for respective area under the curve of chromatogram, the calibration was established using standard mixture of methane premixed carbon dioxide of concentration of 250 ppm and 350 ppm, respectively. The resulting area under the curve was 20520 ppm for methane and 28730 ppm for carbon dioxide. Accordingly, the area under the curve for the peaks of AD showed concentration of methane and carbon dioxide to the tune of 67.27 % and 29.80 %, respectively whereas AD-BES indicated concentration of methane and carbon dioxide to the tune of 83.08 % and 15.75 %, respectively. The study of other gases in biogas not considered in a chromatogram. The conventional AD derived biogas from cow dung reported to contain 60.29 % methane and the cooked starch releases 85.1% [25].

- *Deviation of ORSAT apparatus and gas chromatographic method for analyzing methane concentration in biogas.* In order to compare the two different methods, i.e., statistical analysis-based method using ORSAT apparatus (reported in earlier publication [21]) and gas chromatographic (GC) method for analyzing methane concentration in the biogas, three sets of experimental data were considered.

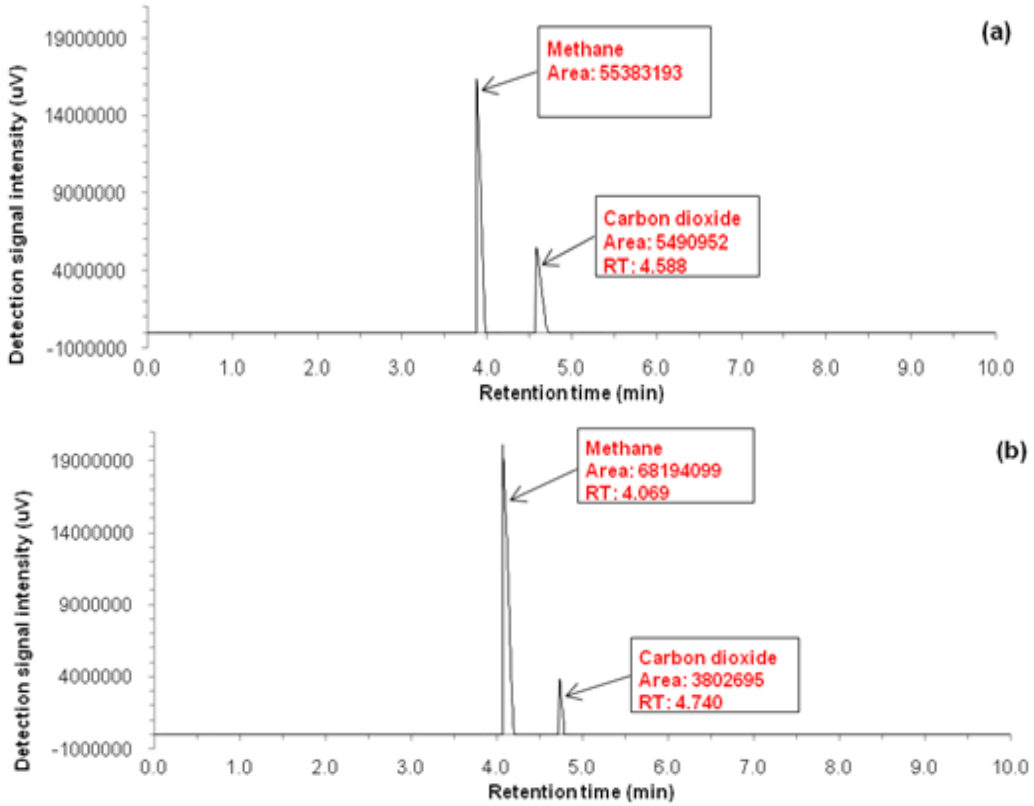

Figure 3. Chromatograms of biogas produced from (a) Only- AD and (b) AD-BES

Out of three data, one set of experiment using ORSAT apparatus method, AD-BES showed concentration of methane and carbon dioxide to the tune of 81.5 v/v% and 15.5 v/v %, respectively, whereas, the chromatographic study showed concentrations of methane and carbon dioxide to the tune of 83.08 % and 15.75 %, respectively. Thus, negligible deviation in the concentration of the two major gases using two different methods was observed, i.e. deviation of 1.66 % for methane and 2.79 % in carbon dioxide. Comparison between these two methods refereed for three sets of experiments.

Characterization of the bioslurry

Table 1. Characteristics of bioslurry obtained from AD-BES and only-AD digesters

Characteristics	Only-AD	AD-BES	% Change
pH	6.7	7.5	10.67
Water, %	89.0	92.1	3.37
Total solids, %	9.5	8.7	-9.20
Volatile solids, %	8.75	7.45	-17.45
C:N ratio	10.08	9.13	-10.41

Table 1 shows the characteristics of bioslurry obtained from two different digesters, i.e., only-AD and AD-BES. It is observed that pH (alkaline nature) of AD-BES-derived bioslurry increased by 10.67%. Improvement in solubility of phosphate and potassium concentration in the bioslurry of AD-BES is believed to be responsible for such increment. It was observed that in contrast to only-AD, bioslurry obtained from AD-BES demonstrated reduced percentage of total solids (9.2%) and volatile solids (17.45%). Such a reduction occurred due to the improvement in decomposition of fatty acids and total ammonium nitrates of the digester inoculum in BES. Some authors reported that solids consisting of manure in the digester were consumed more effectively for biogas generation and mineralization of organic carbon during the operation of AD-BES, leading to increased volume of biogas and methane concentration [26]. A similar reason was demonstrated for the reduction in TS and VS in a bioslurry obtained from AD-BES operated for treatment of sewage [27]. The AD-BES boosts the conversion of digester inoculum. Also, improvement in retention of nitrogen in bioslurry is believed to be responsible for reduction in C/N ratio by 10.41%. In contrast to AD, the bioslurry obtained from AD-BES has lower carbon-to-nitrogen ratio. The acceleration of the nitrogen mineralization process is to be responsible for such a change [28].

Nutrient composition of the bioslurry

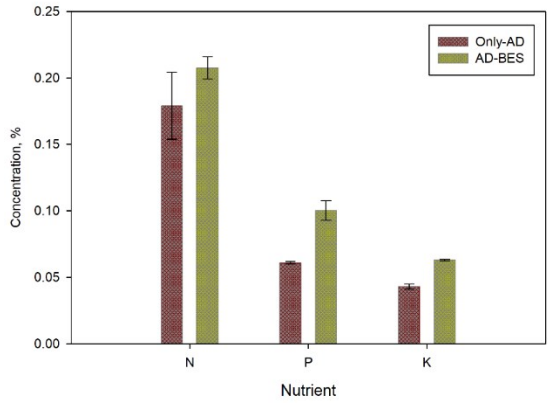

Figure 4, NPK content of bioslurry obtained from AD-BES and only-AD digesters

As shown in Figure 4, in contrast to AD, the bioslurry obtained from AD-BES demonstrated significant improvement in concentration of nutrients such as N, P and K. The nitrogen content of bioslurry increased by 14%, attributed to mineralization of complex organic nitrogen compounds to ammonium ion (NH_4^+) [29, 30]. As shown in equations 2 and 3 the ammonium ion is assumed to be oxidized through oxidizing bacteria at the anode surface of AD-BES producing nitrate (NO_3^-) followed by releasing nitrogen in the bioslurry [31, 32].

$$NH_4^+ + 2O_2 \rightarrow NO_3^- + H_2O + 2H^+ \quad \ldots(2)$$

$$2NO_3 + 10e + 10H^+ \rightarrow N_2 + 2OH + 4H_2O \quad \ldots(3)$$

During the anaerobic digestion process, phosphorus and potassium in the digestate are retained in the bioslurry [33]. The inorganic phosphate remains in the bioslurry, whereas the solid phase of the digestate contains both inorganic and organic phosphate [34]. The phosphorus concentration of the bioslurry from AD-BES increased by 37.04% compared to conventional only-AD. The remarkable improvement in the concentration of phosphate was due to the electrochemical precipitation of inorganic phosphate in the form of hydrate of magnesium ammonium phosphate ($MgNH_4PO_4 \cdot 6H_2O$) [35]. Upon further conversion of such a hydrate, it produces phosphate in the aqueous phase, which resulted in increased concentration of phosphate in the bioslurry of AD-BES. In the case of AD-BES, the concentration of total potassium in the bioslurry was by 19.26 % higher compared to conventional only-AD. The pH (alkaline nature) of the bioslurry is also believed to be responsible for the improvement in solubility of phosphate and potassium in the bioslurry of AD-BES. Thus, overall nutrientx in terms of nitrogen, phosphorus and potassium (NPK) were improved by an average of 28% using AD-BES.

- *Comparative energy requirement of AD-BES and other conventional methods for methane enrichment.* The study showed that for the production of 1 m³ of biogas enriched with 83% methane concentration, the energy requirement was 0.085 kWh (calculated from equation 1) at the supplied voltage of 0.3 V (current density of 0.34 mA/cm^2). As shown in Table 2, the energy required for AD-BES was lower by 43-90% when compared to conventional biogas production methods. This suggests a considerable improvement in energy efficiency using the AD-BES technique. The study is confined to laboratory-scale experiments, meaning real-world applications might show different results. The further research to explore these energy requirements and the potential of AD-BES on a larger scale will be the future scope of work.

Table 2. Comparative energy requirements (kWh) for AD-BES and other conventional methods for methane enrichment

Method	Energy requirement for 1 m^3 biogas generation (kWh)
AD-BES	(0.016 - 0.085) This study
Chemical absorption	(0.05 - 0.25) [36]
Membrane technology (gas/gas or gas/liquid)	(0.2 - 0.38) [37]
Pressure-swing absorption	(0.16 - 0.43) [36]
Absorption (water scrubbing)	(0.2 - 0.5) [36]
Cryogenic separation	(0.42 - 1.0) [37]

CONCLUSION

The results of the statistical analysis-based method using ORSAT apparatus and gas chromatographic analysis for determination of methane and carbon dioxide concentration in biogas are in agreement with each other showing a marginal deviation between the two methods for methane and carbon dioxide in the range of 1.66 % and 2.79%, respectively. The comparative study of bioslurry characteristics resulting from the two digesters, i.e., only-AD and AD-BES, showed that in contrast to only-AD, AD-BES-derived bioslurry demonstrated a significant increase in nitrogen, phosphorus and potassium concentrations (14.29%, 37.04% and 19.26%, respectively). Apart from this, it showed increment in pH and reduction in total solid, volatile solid, C:N ratio. Moreover, the energy requirement (kWh) of AD-BES demonstrated a noteworthy

reduction (by 43-90%) as compared to conventional enrichment methods. The results showed that AD-BES significantly enriched nutrients of bioslurry, improved concentration of methane in biogas at lower energy requirement.

Acknowledgement: *We would like to acknowledge the analytical support by BEIL Infrastructure Limited Ankleshwar, Gujarat, India.*

Declaration: *The authors do not have conflicts of interest to declare that are relevant to the content of this article.*

Funding: *The authors did not receive support from any organization for the submitted work.*

Conflicts of interest/Competing interests*: Not applicable.*

REFERENCES

1. S. D. V. Satyanarayana, *Journal of Biofertilizers & Biopesticides*, **3**(4), (2012). https://doi.org/10.4172/-2155-6202.1000124
2. H. Willer, J. Trávníček, S. Schlatter, The world of organic agriculture. Statistics and emerging trends, Research Institute of Organic Agriculture (FiBL), Frick, and IFOAM-Organics International, Bonn, 2024, p. 1. http://www.organicworld.net/-yearbook/yearbook-2024.html (Accessed 10 Mar 2024)
3. A. H. Bhatt, L. Tao, *Bioengineering*, **7**(3), 74 (2020). https://doi.org/10.3390/bioengineering7030074
4. M. R. Shaibur, H. Husain, S. H. Arpon, *Current Research in Environmental Sustainability*, **3**, 100026 (2021). https://doi.org/10.1016/j.crsust.2021.100026
5. F. Lü, Z. Wang, H. Zhang, L. Shao, P. He, *Bioresource Technology*, **333**, 125196 (2021). https://doi.org/10.1016/j.biortech.2021.125196
6. W. Peng, F. Lü, L. Hao, H. Zhang, L. Shao, P. He, *Bioresource Technology*, **297**, 122485 (2020). https://doi.org/10.1016/j.biortech.2019.122485
7. A. Yasar, S. Nazir, A. B. Tabinda, M. Nazar, R. Rasheed, O.M. Afzaal, *Renewable Energy*, **108**, 19 (2017). https://doi.org/10.1016/j.renene.2017 02.044
8. F. Lü, Z. Wang, H. Zhang, L. Shao, P. He, *Bioresource Technology*, **333,** 125196 (2021) .https://doi.org/10.1016/j.biortech.2021.125196
9. K. Chojnacka, *Biomass Conversion and Biorefinery*, **13,** 14359 (2023) .https://doi.org/10.1007/s13399023-04639-2
10. N. Wang, D. Huang, C. Zhang, M. Shao, Q. Chen, J. Liu, & Q. Xu, *Science of the Total Environment*, **794**, 148785 (2021). https://doi.org/10.1016/j.scitotenv.2021.148785
11. Y. Chen, W. Hu, Y. Feng, S. Sweeney, *Renewable and Sustainable Energy Reviews*, **39,** 679 (2014). https://doi.org/10.1016/j.rser.2014.07.119
12. M. Zubair, S. Wang, P. Zhang, J. Ye, J. Liang, M. Nabi, & Y. Cai, *Bioresource Technology*, **301,** 122823 (2020). https://doi.org/10.1016/j.biortech.-2020.122823
13. J. Lu, L. Jiang, D. Chen et al. *Agriculture, Ecosystems and Environment,* **146**(1), 13 (2012). https:// doi.org/10. 1016/j.agee.2011.10.011
14. X. Zheng, J. Fan, L. Xu, J. Zhou, *PLoS One*, **12**(1), e0170491 (2017). https:// doi. org/ 10. 1371/ journal. pone. 01704 91
15. S. Hazarika, M. J. Barooah, P.K. Dutta, P. Rajkhowa, Enriched biogas slurry: a potential source of nutrients for organic farming, *Akshay Urja*, **26** (2015).
16. K. Koirala, Characterization of ammonia volatilization from liquid dairy manure. PhD. Thesis. Department of Biological Systems Engineering, Washington State University, Washington, 2013.
17. K. Güngör, K. G. Karthikeyan, *Bioresource Technology.* **99**(2)**,** 425 (2008). https://doi.org/ 10.1016/j.biortech.2006.11.049.
18. K. Möller, T. A. Müller, *Eng. Life. Sciences,* **12**, 242 (2012). https://doi.org/10.1002/elsc. 201100085.
19. T. Mdlambuzi, P. Muchaonyerwa, M. Tsubo, M. E. Moshia, *Heliyon*, **7**(5) (2021) .https://doi.org/10.1016/j.heliyon.2021.e07077
20. D. Casini, T. Barsali, A. M. Rizzo, D. Chiaramonti, *Biomass Conversion and Biorefinery*, **11**(6), 2271 (2021). https://doi.org/10.1007/s13399-019-00482-6
21. H. M. Jariwala, Y. C. Rotliwala, *Materials Today: Proceedings*, **57**, 1827 (2022). https://doi.org/ 10.1016/j.matpr.2022.01.024
22. APHA, AWWA, WEF, Standard Methods for Examination of Water and Wastewater, 22nd edn., American Public Health Association, Washington, 2012.
23. B. A. Chaka, A. M. Osano, J. K. Maghanga, M. M. Magu, *Advances in Agriculture*, **2020**(8), 1 (2020). https://doi.org/10.1155/2020/4526485
24. E. K. Orhorhoro, P. O. Ebunilo, G. E. Sadjere, *American Journal of Modern Energy*, **3** (6), 131 (2017). DOI:10.11648/j.ajme.20170306.13
25. A. Wellington, L. D. Baraza, M. Mageto, K. F. Orori, *Phys Sci Int J.,* **16**(4), 1 (2017). https:// doi. org/ 10. 9734/ PSIJ/ 2017/ 38559 20.
26. A. Kumar, L. M. Verma, S. Sharma, et al. *Biomass Conv. Bioref.* **13,** 13729 (2023). https://doi.org/ 10.1007/s13399-021-02215-0
27. M. Ahmadi-Pirlou, T. Mesri Gundoshmian, *J. Mater. Cycles Waste Manag.* **23**, 1938 (2021). https://doi.org/10.1007/s10163-021-01264-x
28. M. Hermassi, C. Valderrama, O. Gibert, N. Moreno, X. Querol, N. H. Batis, J. L. Cortina, *Science of the Total Environment*, **599,** 422 (2017). https://doi.org/ 10.1016/j.scitotenv.2017.04.140
29. F. Tambone, V. Orzi, G. D'Imporzano, F. Adani, *Bioresource Technology*, **243,** 1251 (2017). https: //doi.org/10.1016/j.biortech.2017.07.130
30. M. O. Doyeni, U. Stulpinaite, A. Baksinskaite, S. Suproniene, V. Tilvikiene, *Plants*, **10**(8), 1734 (2021). https://doi.org/10.3390/plants10081734
31. H. Wang, H. Luo, P. H. Fallgren, S. Jin, Z. J. Ren, *Biotechnology Advances*, **33**(3-4), 317 (2015). https://doi.org/10.1016/j.biotechadv.2015.04.003

32. A. Nasir, M. U. Khalid, A. Munir, S. Anwar, *Journal of Research in Engineering and Technology*, **1**, 81 (2015).
33. T. A. Sogn, I. Dragicevic, R. Linjordet, T. Krogstad, V. G. Eijsink, S. Eich-Greatorex, *International Journal of Recycling of Organic Waste in Agriculture*, **7,** 49 (2018). https://doi.org/10.1007/s40093-017-0188-0
34. B. Li, K. Dinkler, N. Zhao, M. Sobhi, W. Merkle, S. Liu, J. Guo, *Science of the Total Environment*, **737,** 140234 (2020). https://doi.org/10.1016/j.scitotenv.2020.140234
35. F. Fischer, C. Bastian, M. Happe, E. Mabillard, N. Schmidt, *Bioresource Technology*, **102**(10), 5824 (2011). https://doi.org/10.1016/j.biortech.2011.02.089
36. R. Kapoor, P. Ghosh, M. Kumar, V. K. Vijay, *Env. Sci. Poll. Res.* **26,** 11631 (2019). https://doi.org/10.1007/s11356-019-04767-1
37. F. Bauer, C. Hulteberg, T. Persson, D. Tamm, Svenskt Gastekniskt Center AB, 2013. 82 p. http://www.sgc.se/ckfinder/userfiles/files/SGC270.pdf

Acknowledgement to Reviewers for vol. 56 (2024)

The Editors of Bulgarian Chemical Communications would like to take this opportunity to thank you for the effort and expertise that you contributed to reviewing, without which it would be impossible to maintain the high standards of our journal:

A

A. Decheva
A. Georgieva
A. Kijo-Kleczkowska
A. Momchilov
A. Ouasri
A. Stoyanova
A. Ugrinov

B

B. Dzhiembaev
B. Georgieva
B. Stefanov
B. Todorov
B. Toshev
Bl. Yovkova

C

Ch. Chilev

D

D. Antonova
D. Christova
D. Dzhonova
D. Kolev
D. Minkovska
D. Nikolova
D. Sakar
D. Todorovski
D. Vladikov

E

E. Georgieva
E. Ivanova
E. Slavcheva
E. Cherneva

G

G. Borisov
G. Gergov
G. Pekov

H

Hr. Nichev

I

I. Balchev
I. Doytchinova
I. Grabchev
I. Ion
I. Karadjova
I. Prokopov
I. Tsacheva

J

J. Kolev
J. Krzywanski
J. Zaharieva

K

K. Ivanova
K. Praveen

M

M. Abrashev
M. Argirova
M. Georgieva
M. Kondeva
M. Milanova
M. Rangelov
M. Petrov
M. Tsvetkov
M. Velikova
M. Yelubay

N

N. Grozev
N. Koseva
N. Mincheva
N. Penov
N. Trendafilova

P

Pl. Petkov
P. Petrov
P. Petrova
P. Vasileva

R

R. Bryaskova
R, Stoyanova

S

S. Đorđević
S. Kolev
S. Rabadzhiyska
S. Raikumar
St. Shilev
S. Vasilev

T

T. Hristova-Vasileva
T. Manasieva
T. Paunova
T. Veselinov
Ts. Zahariev

V

V. Beschkov
V. Dimitrov
V. Kňazovická
V. Lovchinov
V. Lyubomirova
V. Simeonov
V. Slaveykova
V. Tsankova

Y

Yu. Tumbarski
Y. Yalcin-Gurkan

Instructions about Preparation of Manuscripts

General remarks: Manuscripts are submitted in English by e-mail. The text must be prepared in A4 format sheets using Times New Roman font size 11, normal character spacing. The manuscript should not exceed 15 pages (about 3500 words), including photographs, tables, drawings, formulae, etc. Authors are requested to use margins of 2 cm on all sides.

Manuscripts should be subdivided into labelled sections, e.g. INTRODUCTION, EXPERIMENTAL, RESULTS AND DISCUSSION, etc. **The title page** comprises headline, author(s)' names and affiliations, abstract and key words. Attention is drawn to the following:

a) **The title** of the manuscript should reflect concisely the purpose and findings of the work. Abbreviations, symbols, chemical formulae, references and footnotes should be avoided. If indispensable, abbreviations and formulae should be given in parentheses immediately after the respective full form.

b) **The author(s)'** first and middle name initials and family name in full should be given, followed by the address (or addresses) of the contributing laboratory (laboratories). **The affiliation** of the author(s) should be listed in detail (no abbreviations!). The author to whom correspondence and/or inquiries should be sent should be indicated by an asterisk (*) with e-mail address.

The abstract should be self-explanatory and intelligible without any references to the text and containing up to 250 words. It should be followed by keywords (up to six).

References should be numbered sequentially in the order, in which they are cited in the text. The numbers in the text should be enclosed in brackets [2], [5, 6], [9−12], etc., set on the text line. References are to be listed in numerical order on a separate sheet. All references are to be given in Latin letters. The names of the authors are given without inversion. Titles of journals must be abbreviated according to Chemical Abstracts and given in italics, the volume is typed in bold, the initial page is given and the year in parentheses. Attention is drawn to the following conventions: a) The names of all authors of a certain publications should be given. The use of "et al." in the list of references is not acceptable; b) Only the initials of the first and middle names should be given. In the manuscripts, the reference to author(s) of cited works should be made without giving initials, e.g. "Bush and Smith [7] pioneered...". If the reference carries the names of three or more authors it should be quoted as "Bush et al. [7]", if Bush is the first author, or as "Bush and co-workers [7]", if Bush is the senior author.

Footnotes should be reduced to a minimum. Each footnote should be typed double-spaced at the bottom of the page, on which its subject is first mentioned. **Tables** are numbered with Arabic numerals on the left-hand top. Each table should be referred to in the text. Column headings should be as short as possible but they must define units unambiguously. The units are to be separated from the preceding symbols by a comma or brackets. Note: The following format should be used when figures, equations, etc. are referred to the text (followed by the respective numbers): Fig., Eqns., Table, Scheme.

Schemes and figures. Each manuscript should contain or be accompanied by the respective illustrative material, as well as by the respective figure captions in a separate file. As far as presentation of units is concerned, SI units are to be used. However, some non-SI units are also acceptable, such as °C, ml, l, etc. Avoid using more than 6 (12 for review articles) figures in the manuscript. Since most of the illustrative materials are to be presented as 8-cm wide pictures, attention should be paid that all axis titles, numerals, legend(s) and texts are legible.

The authors are required to submit the text with a list of three individuals and their e-mail addresses that can be considered by the Editors as potential reviewers. Please note that the reviewers should be outside the authors' own institution or organization. The Editorial Board of the journal is not obliged to accept these proposals.

The authors are asked to submit **the** final text (after the manuscript has been accepted for publication) in electronic form by e-mail. The main text, list of references, tables and figure captions should be saved in separate files (as *.rtf or *.doc) with clearly identifiable file names. It is essential that the name and version of the word-processing program and the format of the text files is clearly indicated. It is recommended that the pictures are presented in *.tif, *.jpg, *.cdr or *.bmp format. The equations are written using "Equation Editor" and chemical reaction schemes are written using ISIS Draw or ChemDraw programme.

EXAMPLES FOR PRESENTATION OF REFERENCES

REFERENCES

1. D. S. Newsome, Catal. Rev.–Sci. Eng., 21, 275 (1980).
2. C.-H. Lin, C.-Y. Hsu, J. Chem. Soc. Chem. Commun., 1479 (1992).
3. R. G. Parr, W. Yang, Density Functional Theory of Atoms and Molecules, Oxford Univ. Press, New York, 1989.
4. V. Ponec, G. C. Bond, Catalysis by Metals and Alloys (Stud. Surf. Sci. Catal., vol. 95), Elsevier, Amsterdam, 1995.
5. G. Kadinov, S. Todorova, A. Palazov, in: New Frontiers in Catalysis (Proc. 10th Int. Congr. Catal., Budapest (1992), L. Guczi, F. Solymosi, P. Tetenyi (eds.), Akademiai Kiado, Budapest, 1993, Part C, p. 2817.
6. G. L. C. Maire, F. Garin, in: Catalysis. Science and Technology, J. R. Anderson, M. Boudart (eds.), vol. 6, Springer Verlag, Berlin, 1984, p. 161.
7. D. Pocknell, GB Patent 2 207 355 (1949).
8. G. Angelov, PhD Thesis, UCTM, Sofia, 2001, pp. 121-126.
9. JCPDS International Center for Diffraction Data, Power Diffraction File, Swarthmore, PA, 1991.
10. CA 127, 184 762q (1998).
11. P. Hou, H. Wise, J. Catal., in press.
12. M. Sinev, private communication.
13. http://www.chemweb.com/alchem/articles/1051611477211.html.

Texts with references which do not match these requirements will not be considered for publication!!!

CONTENTS